Student thesis series INES nr 499

Interpreting and composing SAGE II-III satellite data with a cloud algorithm for stratospheric aerosols

Carl Svenhag

2020
Department of
Physical Geography and Ecosystem Science
Lund University
Sölvegatan 12
S-223 62 Lund
Sweden

Carl Svenhag (2020).
Interpreting and composing SAGE II-III satellite data with a cloud-algorithm for stratospheric aerosols.
Tolkning och arrangering av SAGE II-III satellitdata med en molnalgoritm för stratosfäriska aerosoler.
Master degree thesis, 30 credits in *Atmospheric Science and Biochemical cycles*
Department of Physical Geography and Ecosystem Science, Lund University

Level: Master of Science (MSc)

Course duration: *January* 2019 until *January* 2020

Disclaimer

Interpreting and composing SAGE II-III satellite data with a cloud-algorithm for stratospheric aerosols

---

Carl Svenhag

Master thesis, 30 credits, in *Atmospheric Science and Biochemical Cycles*

Johan Friberg
Lund University

Exam committee:
Thomas Holst, Lund University
Vaughan Phillips, Lund University

Abstract

Understanding and quantifying radiative effects by high air-bound particles is a significant component to further develop the climate models we use today for understanding past and future climate change (IPCC, 2013). In this study I seek to provide observations and understanding of sulphuric aerosols bound in the stratosphere from natural and possibly anthropogenic sources. Respectively draw attention to where the aerosols are located and why. The most intensive source of additional stratospheric aerosol loads stems from volcanic eruptions and in June 1991 Mt Pinatubo injected over 20 tonnes of SO_2 into the troposphere and subsequently high up in the stratosphere. The climate impact of resulting Pinatubo aerosols is considered one of the largest stratospheric disruptions in the 20th century (McCormick, 1995). The study of forest fire aerosols being lunged into the stratosphere is an uncertain field which may carry more weight to our global radiative budget than previously thought. The observation of these effect is made possible through the SAGE project which have been observing light-scattering and absorption of stratospheric compounds since 1979. SAGE II (1984–2005) and SAGE III (2017-) are included in this research with a developed cloud algorithm, and these methods and results are compared to previous studies for mapping stratospheric aerosols.

Keywords: Atmospheric Science, Satellite Observations, Aerosol Optical Depth, SAGE, Cloud Algorithm, Stratospheric Aerosols, Radiative Forcing.

Sammanfattning

Tolkning och kvantifiering av strålningseffekter pga. atmosfäriska partiklar är en signifikant del av IPCC's (2013) modellering av hur tidigare klimat förändrats och hur förändringar i framtiden kommer se ut. I den här studien vill vi strukturera och analysera observationer av huvudsakligen svavelpartiklar positionerade i stratosfären från naturliga och möjligtvis mänskliga källor, med hänvisning till var och varför de finns där. Vulkaniska utbrott är den största källan till naturligt höga aerosolkoncentrationer i stratosfären. Juni 1991 exploderade vulkanen Pinatubo i Indonesien och slungade kring 20 ton svaveldioxid in i atmosfären, med stor omfattning långt in i stratosfären. Effekterna av de resulterande aerosolerna från Pinatubo är uppskattat att vara en av de största klimat-inverkningarna av stratosfäriska partiklar under 1900-talet. Under väldigt stora skogsbränder kan liknande vräkningar av svavel ske upp till stratosfären, och detta är ett relativt glest studieområde men kan möjligtvis ha en viss tyngd i jordens strålningsbalans som är värd at undersöka. Iakttagelser av dessa stratosfäriska fenomen kan tillfogas med hjälp av satellitdata från SAGE II (1984–2005) och SAGE III (2017-), som observerar ljusets spridning och absorbering av olika partiklar i atmosfären. Genom att applicera och jämföra en molnalgoritm, våra resultat och tidigare studier strävar vi efter att kartlägga den stratosfäriska aerosolen för detta tidsintervall.

Acknowledgements

This project is performed to contribute to further study by **Friberg et al. (2018)** on the period 1984–2005 (SAGE II) and 2017–2019 (SAGE III) of stratospheric aerosol analysis and future projects made by our group at the department of nuclear physics at Lund University. From the group I would personally like to thank Johan Friberg, Bengt G. Martinsson, Moa Sporre and Oscar S. Sandvik for their cooperation and contribution to this project.

All figures used in this report from external sources have been cited correspondingly with access consent.

Acronyms and Abbreviations

AOD	Aerosol Optical Depth
ATAL	Asian Tropopause Aerosol Layer
CALIPSO	Cloud-Aerosol Lidar & Infrared Pathfinder Satellite Observation
CCN	Cloud Condensation Nuclei
CDNC	Cloud Droplet Number Concentration
CFCs	Chlorofluorocarbons
CLAES	Cryogenic Limb Array Etalon Spectrometer
ECMWF	European Centre for Medium-Range Weather Forecasts
ERBS	Earth Radiation Budget Satellite
Ext	Extinction coefficient
ExTL	Extratropical Transition Layer
GloSSAC	The Global Space based Stratospheric Aerosol Climatology
HALOE	Halogen Occultation Experiment
ISS	The International Space Station
IPCC	Intergovernmental Panel on Climate Change
LMS	Lower Most Stratosphere
MERRA	Modern-Era Retrospective analysis for Research and Application
NH	Northern Hemisphere
PSC	Polar Stratospheric Cloud
SAGE	Stratospheric Aerosol & Gas Experiment
SH	Southern Hemisphere
TP	Tropopause
T.V.	Thomasson and Vernier (2013)
UTLS	Upper Troposphere & Lower Stratosphere
UV	Ultra Violet
WMO	World Meteorological Organisation

Contents

1. Introduction

The impact Stratospheric Aerosols have on our Earth's climate and energy budget, can be regarded as an important but uncertain field. In particular when glancing at IPCC's (2013) AR5 radiative forcing schematics and their respective *Level of Confidence*. But recognizing that aerosols in the atmosphere are having a significant impact to our weather and climate is not a newly implied discovery. A historic example was when the Laki volcano on Iceland erupted in 1783–1784, and Benjamin Franklin affiliated the excess gas and aerosols from the volcano to be the potential cause of the abnormally cold seasons in Europe that year (Zambri et al. 2019). The extreme natural phenomena by volcanos can change the climate unlike anything else on a global scale. The immense release of energy can force particulate matter high up to the lower stratosphere, and then it could potentially remain there for years to follow. Sulphur dioxide (SO_2) and carbonyl sulphide (OCS) are components in this violent projection from volcanic cascades and can form clouds of aerosol residue in the lower stratosphere consequently (Robock, 2000). These aerosol clouds, generated through series of particle nucleation, accumulation and condensation processes, will serve as an atmospheric parasol in the stratosphere (Wallace and Hobbs, 2006).

As the climate and chemistry in the biosphere have undergone drastic changes since the dawn of the industrial age and one player in this complicated system is the direct aerosol effect. This is the micro-scale process where air-bound aerosols particles inhibit solar radiation from reaching the Earth's surface through absorption and scattering of light. Successively, a result of excess aerosol particles bound in e.g. the stratosphere can be anticipated to have a negative radiative effect to our Earth's energy budget. This implies that added aerosols, from e.g. volcanic eruptions, into the upper atmosphere would be followed by a cooling of the underlying atmosphere and the surface climate (Ahrens, 2008). This does have some exceptions, e.g. the daily visible anthropogenic contrails from aircrafts which is a phenomenon that grants a net positive radiative forcing (climate warming) just like CO_2 and other greenhouse gases. Polar stratospheric clouds (PSC) are another composition of particulate matter occurring in the polar stratosphere, and these acid clouds are also known to influence the atmospheric climate through processes such as radiative forcing and ozone destruction (Ahrens, 2008). Volcanic and other stratospheric aerosol types additionally have indirect effects on the radiation budget when they e.g. descend below the UTLS and can possibly act as additional ice nuclei (IN). As these excess aerosols may contribute to formation of clouds with high cloud ice/droplet number concentrations (CDNC) and possibly reduce cloud ice/droplet sizes. These cloud-characteristics could cause more scattering of incoming sunlight-radiation than a non-aerosol enhanced atmosphere would, this is called the *Twomey effect* (Twomey, 1977). An additional aerosol indirect climate effect for the troposphere include prolong-lived clouds, that would be the result of excess aerosol cloud condensation nuclei (CCN) with smaller droplet size, that potentially fail to reach the threshold mass to precipitate out (Albrecht, 1989). Thereby, finding and compiling the amount of scattering and absorption for

various wavelengths in the whole atmosphere, caused by gases, aerosols and clouds, will be key to determine how our Earth's radiation budget and climate will change over time.

In the fall of 1984, the mission of Stratospheric Atmospheric Aerosol and Gas Experiment II (SAGE II) was launched onboard the Earth Radiation Budget Satellite (ERBS), aiming to collect information on the composition of aerosols, NO_2, water vapor and ozone in the stratosphere. This satellite was sent into orbit 610 kilometres above the Earth surface with a 57° inclination (McCormick, 1987) and after impressive 21 operational years it was decommissioned on October 14, 2005. Five major volcanic eruptions showed observable stratospheric signatures during the SAGE II operational lifetime, El Chichón (1982), Ruiz (Nov. 1985), Kelut (Feb. 1990), Pinatubo (Jun. 1991), Hudson (Aug 1991) and Manam (Jan. 2005), (Bauman et al., 2003; Thomasson and Vernier 2013). The magnitude of Pinatubo far outshined the other three as the 1991 catastrophic eruption in the Philippines was the second largest volcanic eruption in the 20th century. McCormick et al. (1995) stated that the aftermath of Mt Pinatubo cooled the global climate the following years greatly. The successor SAGE III is currently operational onboard the ISS and will continue the employment of stratospheric observation into the new decade. So far two larger eruptions have occurred during the SAGE III ISS project, Ambae (Jul. 2018) and Raikoke (Jul. 2019).

2. Background and Theory

2.1 The stratospheric composition

The characteristics and concentrations of aerosols in the atmosphere can vary significantly throughout the vertical profile, and its changing related to various factors, e.g. pressure, temperature and water availability. A layer of air between approximately 17- 20 km, around and above the tropopause, is a known region with high concentrations of sulphuric aerosols, with diameters ranging from ~0.1 to 2 µm (Aitken-accumulation mode) called the *stratospheric sulphate layer* (Wallace and Hobbs, 2006). The particles in this layer are the result of oxidized sulphur dioxide ($SO_2 \rightarrow SO_3$) mixed with water (H_2O) and form sulphuric acid (H_2SO_4), see Wallace and Hobbs (2006) for full chemical computation. This high-sulphur layer is included in parts of the lower most stratosphere (LMS) which is referred to in this study and by Friberg et al. (2018) as the layer between the tropopause and the 380 Kelvin potential temperature (isentropic) surface. In the LMS, high-sulphur downwelling air from the stratosphere is mixed with air from the upper troposphere changing the aerosol composition of this layer due to the recurring exchange in the extratropical transition layer, or *ExTL* (Gettelman et al. 2011). A secondary thin layer of the stratosphere, related to the lower Brewer-Dobson circulation, is estimated to be in the range of 380–470 K isentropic surfaces (Fueglistaler et al., 2009; Lin and Fu, 2013). This includes the mentioned high-sulphate layer and is defined as one of the stratospheric layers in Friberg et al. (2018) and our methodology. Lastly, Friberg et al. (2018) defines a layer with the *tropical pipe* from the 470 K isentropic surface to a near-*particle free* altitude (~35 km). Here, only significantly large sources of energy, generally associated with major volcanic eruptions, could transport high concentrations of aerosol from the troposphere to these upper parts of the stratosphere.

A calculation of potential temperature for an ideal gas, from Holton and Hakim (2013) and applied for defining mentioned isentropic surfaces can be given as

$$\theta = \mathrm{T}\left(\frac{\mathrm{p_s}}{\mathrm{p}}\right)^{\frac{\mathrm{R}}{\mathrm{cp}}} \qquad (1)$$

Where *eq.1* gives a potential temperature of an airmass with temperature (*T*) and pressure (*p*) relative to surface pressure (p_s) and specific heat constant c_p (at constant pressure = 1004 $J \cdot kg^{-1} \cdot K^{-1}$) and assumed gas constant for dry air *R* (287 $J \cdot kg^{-1} \cdot K^{-1}$). These needed parameters are available in the v.7.0 SAGE II data set, but they are produced through modelling and are not real observed values of temperature and pressure.

2.2 SAGE

The enduring stratospheric aerosol and gas satellite experiments SAGE I through III have pioneered on four different satellites throughout history, from the Explorer 60 (SAGE I 1979–1981), the ERBS (SAGE II), and lastly SAGE III passing from the Russian Meteor-3M satellite (2002–2007) to the International Space Station (ISS) sampling from 2017 to present day (Thomasson et al. 2018). With focus on SAGE

II in this project, the four working wavelength channels included in the version 7.0 datasets are 386 nm, 452 nm, 525 nm, 1028 nm (NASA, 2019). The SAGE II measurements of stratospheric ozone depletion were a foundation for the 1987 inferred Montreal Protocol, which inhibited release of CFCs by industrialized countries.

The method of data-capturing used by the SAGE instruments differs significantly from that of concurrent Lidar surveying which collects backscattering of produced wavelengths, sweeping in a practically perpendicular direction to that of SAGE. Alternatively, SAGE is using the natural source of light from the face of the Sun passing through the atmosphere viewing sunsets and sunrise events, referred to as solar occultation measurements, see Fig. 2.1 for illustration. The SAGE instrument method receives an image of the light travelled through the atmosphere and how much of this light that may have been scattered and/or absorbed in its path. A good background radiation profile is easy to compose for SAGE as the instrument can observe the sun through space before or after collecting a sweep, called *self-calibrated* as referred in Thomasson et al. (2008). The latest SAGE III instrument has additionally included *Lunar occultation*, which measures intensity of reflected radiation coming from the Moon to improve the resulting atmospheric profile accuracy (Yue et al. 2005). The SAGE III on ISS however, have a lower orbital inclination (51.5°) than SAGE II (57°) resulting in SAGE II capturing higher latitudes (up to ~80°N/S) and constricting SAGE III inside latitudes of only ~60° north and south, but with higher frequency of data.

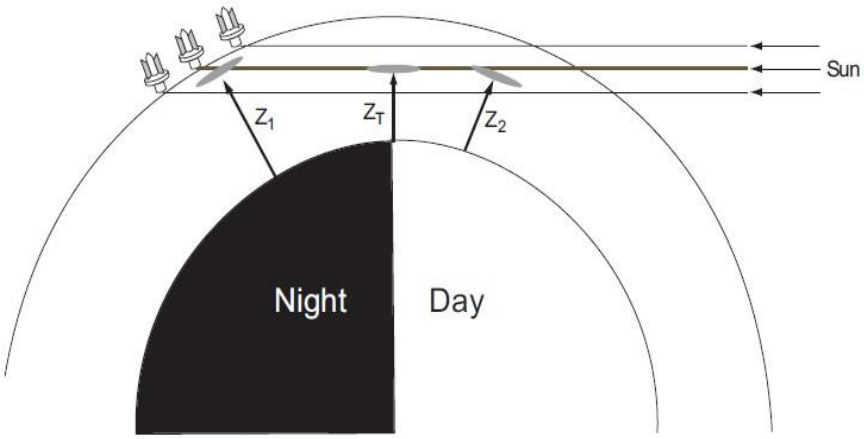

Figure 2.1: Simplified SAGE II measurement geometry where Z_T (called the tangent point) is the target air mass profile, Z_1 and Z_2 illustrates how clouds may interfere in the line of sight of the Instrument for the intended tangent point, illustration taken from Thomasson and Vernier (2013).

To produce a vertical profile however, a so-called *onion peeling* method has been applied by the SAGE computation to calculate the intended vertical layer properties of the tangent position (Z_t in Fig. 2.1) down to the second decimal of a coordinate degree (Damadeo et al. 2013). This generates several problems as interference in one layer can affect the calculated data in a layer below as illustrated in Fig. 2.1. The SAGE calculations must also consider the refraction in the atmosphere when calculating a

tangent altitude (Z_t in Fig. 2.1), so the lines of light seen in Fig. 2.1 are not actually passing through the atmosphere in a straight path but more curvaceous towards the earth (Thomasson et al. 2008). In the year 2000 SAGE II experienced an instrument malfunction resulting in that the number of total measurements were reduced by 50% the remaining five years.

2.3 Atmospheric optics

Describing the amount of light that is scattered and/or absorbed through the air, the unitless parameter of extinction, or loss of light, is utilized for observing how these photons with different wavelengths (λ) behave in the atmosphere. The sunlight that is observed by the SAGE instrument fall within wavelengths of 300-1000 nm which include the visible spectrum of light. Extinction of these wavelengths in the atmosphere by gases and particles will change depending on various factors such as e.g. intensity of the incoming light, the concentration of the present particles/gases and their size or shape (Kent et al. 1991). Quantifying the amount of light that is extinct over a distance gives us the extinction coefficient in units of km^{-1} (Wallace and Hobbs, 2006).

A relationship between the aerosol-size and the scattered photon-wavelength can in simple form be explained through three types of scattering, called Rayleigh, Mie and Optical scattering. For Rayleigh scattering, the incident light wavelength is significantly larger than the radius of the particle or molecule (r) it interacts with and a defined dimensionless scattering efficiency (Q_λ) will change following the relationship $Q_\lambda \propto \lambda^{-4}$ (Wallace and Hobbs 2006). The Rayleigh scattering, with $1 \gg 2\pi r/\lambda$, distributes light evenly in all directions (Wallace and Hobbs, 2006). This form of scattering is thereby what we are witnessing from a clean atmosphere that is free of e.g. clouds, dust and smoke. However, the scattering efficiency of Rayleigh scattering is significantly lower than that of Mie and Optical scattering.

When the sky is perceived hazy and grey-whiteish, it could be the result of Mie scattering caused by the mentioned larger particles in the atmosphere, where $1 \leq 2\pi r/\lambda$ and the scattering of all wavelengths is more efficient, making the sky appear hazier (Wallace and Hobbs 2006). The relationship between Q_λ and particle radius to wavelength ratio in this case is more intricate and defined through a decrementing cosine-fluctuating relationship, also referred to as *Mie Theory* (Wallace and Hobbs, 2006). Lastly optical scattering is occurring when $2\pi r/\lambda \gg 1$ and all wavelengths are scattered equally with a scattering efficiency converged to a value of ~2 (Wallace and Hobbs 2006). This type of scattering is what e.g. makes cloud white, as the cloud droplets and ice crystals can coagulate and condense to sizes over 1 cm in diameter (Ahrens, 2008).

Some aerosols and gases, along with cloud droplets and ice crystals, have a significant absorption that influence the total extinction. The radiative absorption by aerosols and gases are related to an intricate relationship between the energy of the incident photon and the molecular structure and/or vibration of the absorber (Wallace and Hobbs, 2006). An excess of potential energy will be emitted again almost instantaneously after

absorption, conceivably in a new form (different wavelength) depending on if/how the structure of the molecule/particle may have changed. A good example of this process are the characteristics of our ozone layer in the stratosphere, where O_3 is absorbing shortwave UV radiation, splitting its molecular structure and releasing thermal energy giving the stratosphere its vertically increasing temperature profile. Likewise, some large volcanic soot aerosols in the atmosphere can have a significant amount of absorption that will in turn cause warming on its ambient surroundings by releasing its excess energy as heat (Ahrens, 2008).

Calculations made by Yue et al. (1986) using Rayleigh and Mie theory with intricate analysis defined an empirical relationship between the aerosol extinction coefficients of SAGE wavelength bands ~0.5 μm and 1 μm. They were generally observed, using SAGE II data, to coincide within a range of 525 nm/1020 nm ratio of 2 to 5 for the background aerosol (Kent et al. 1991). They also concluded that the extinction coefficient for both wavelengths will be significantly higher (up to ~10^2 in magnitude) when the light is obstructed by clouds and the ratio for 525/1020 nm would be ~1 (Kent et al. 1991).

The unitless parameter commonly used to illustrate aerosol influence is aerosol optical depth (AOD) and is defined simply as the extinction coefficient integrated over the distance of interest, in our case through the various layers of the stratosphere. However, computing a global stratospheric AOD by using zonal values (AOD_φ) requires the use of a weighted mean (AOD_W in Eq. 2), as each latitude (φ) have a distinct sized grid of the stratosphere. This is easily visualized when observing the meridian lines on a globe.

$$\mathrm{AOD}_W = \frac{\sum(\mathrm{AOD}_\varphi * \cos(\varphi))}{\sum \cos(\varphi)} \tag{2}$$

For Eq. 2 and our results of a global latitude-weighted mean, with the assumption that that the Earth is a perfect sphere in this case.

2.4 SAGE II 1993 cloud classification

Kent et al. (1991) and Yue et al. (1986) illustrate and describe the relationship of 1020 nm and 525 nm extinction coefficients to aerosol scattering mentioned above, to then distinguish clouds from aerosol signatures in the SAGE II data. Initially for their classification method, Kent et al (1993) creates an additional coordinate system (see Eq. 3 and Eq. 4), which excludes all values where the 1020 nm (X) extinction coefficient is larger than the 525 nm. Thereafter they can classify datapoints from a scatterplot of SAGE II data taken from a specific height, time-period and latitude band and add it accordingly into Fig. 2.2. Each angle θ (in degrees) will contain a quantity of values, and the angle with the highest density of datapoints θ_m be used to derive where the separation line for classification cross the *1.0 μm Extinction* axis (x-axis in Fig. 2.2) is placed, see Fig. 4.3 for illustrated application of the Kent method. The standard deviation of a normal distribution from datapoints containing the aerosol centroid angle is labelled as σ in Kent et al. (1993).

$$X' = (X * \sin\theta - Y * \cos\theta)/\sin(\theta - 45°) \quad (3)$$

$$Y' = (Y * \cos 45° - X * \sin 45°)/\sin(\theta - 45°) \quad (4)$$

Final equation for the cloud/aerosol categorization line (seen in Fig. 4.3*)* is given as

$$Y = \left(X - \frac{X_0' + 2\sigma}{\sqrt{2}}\right)\tan\theta_m \quad (5)$$

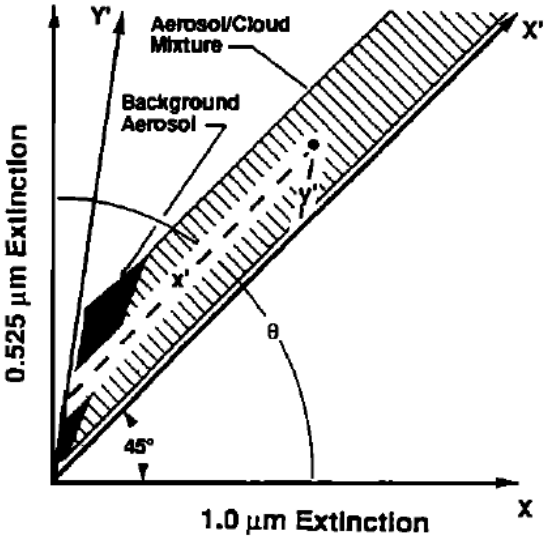

Figure 2.2: Illustration of how extinction coefficients are classified depending of the 0.525 μm vs 1.020 μm value, with a X' axis placed on the ratio-1 line, and Y' as given in Eq**.** 4. θ is the angle relative to the x-axis. Figure is acquired from Kent et al. (1993).

Application of this method can be seen in Kent et al. (1993) and in following sections.

2.5 SAGE II 2013 cloud classification

This related study focuses on the ambigous particulate atmospheric region called the Asian Tropopause Aerosol Layer (ATAL) in the Upper Tropospheric and Lower Stratospheric (UTLS) levels during the SAGE II period of 1989–1990 and 1996–2006 (Thomasson and Vernier 2013). These periods are considered to have much less volcanic atmospheric perturbations compared to excluded stages of SAGE II (eruptions from Ruiz and Pinatubo). Grounded in method by Kent et al. (1993) they similarly use the extinction coefficient relationship of channels 525 nm and 1020 nm to create a suitable cloud mask, I refer to this as the T.V. method in this report. Instead of using an alternative coordination system based on ratio of values/angles in a represented scatter plot, they plot the ratio of 525 nm and 1020 nm directly on the y-axis with a logarithmic 1020 nm extinction coefficient on the x-axis to get a scatter-plot appearance as seen in Fig. 2.3.

The Thomasson and Vernier (2013) equation of cloud/aerosol separation is described as 525nm/1020nm extinction coefficient ratio R as a function of extinction coefficient 1020 nm k seen in Eq.4.

$$R = \frac{aR_c k_c + (1-a)R_a k_a}{ak_c + (1-a)k_a} + \delta \;\; , \; a = \frac{k - k_a}{k_c - k_a} \quad (6)$$

Here R_c represents the R value at the cloud centroid (artificially set to ratio-*1*) and R_a the ratio value at the aerosol centroid which will change, just like the Kent method, for

each selected year, season, altitude and latitude. Accordingly, the $k_c$value they set to constant 10^{-4} km^{-1} and with a varying k_a value like R_a (Thomasson and Vernier 2013). They empirically selected the value for δ to 0.4 which represents the offset in the y-direction from k_c to separate cloud/aerosol values recognizable in Fig. 2.3 (Thomasson and Vernier 2013). This separation line (seen as red in Fig. 2.3) is conjoined with a boundary line (seen as green in Fig. 2.3) which represents a linear cloud/aerosol boundary on the 1020nm extinction coefficient axis given as k_a + $3\Delta k_a$. The Δk_a is defined as the median absolute deviation for 525nm and 1020nm extinction coefficient ratio for values exceeding 3, which they claim to separate primary aerosol from "enhanced" aerosol adequately (Thomasson and Vernier 2013).

The cloud mask in their study (like our new method) is performed for altitudes between 6-20 km as cloud above 20 km altitude are only seen as PSC on high latitudes in the data which are mainly not concerning for Thomasson and Vernier (2013) as they study the tropics. The PSC's will be further questioned in the *Method and Application* of our study, but noted that Thomasson and Vernier (2013) uses a threshold temperature for removing PSC developed by Pitts et al. (2008).

The black dotted *Enhanced Aerosol* line is representing their interpretation of the Kent method which is described in Eq. 7. Instead of computing the original method by Kent et al. (1993) they define the value k_i where the separation line intersects the x-axis (the 1020-nm extinction coefficient axis) in Eq. 7 as *edge of the main aerosol centroid* (Thomasson and Vernier, 2013).

$$\mathrm{R} = \mathrm{m} - \frac{\mathrm{m} * \mathrm{k_i}}{\mathrm{k}} \tag{7}$$

In Eq. 7, *m* and k_i vary correspondingly to k_a and R_a (*eq.4)* in response to season, altitude and latitude (Thomasson and Vernier, 2013).

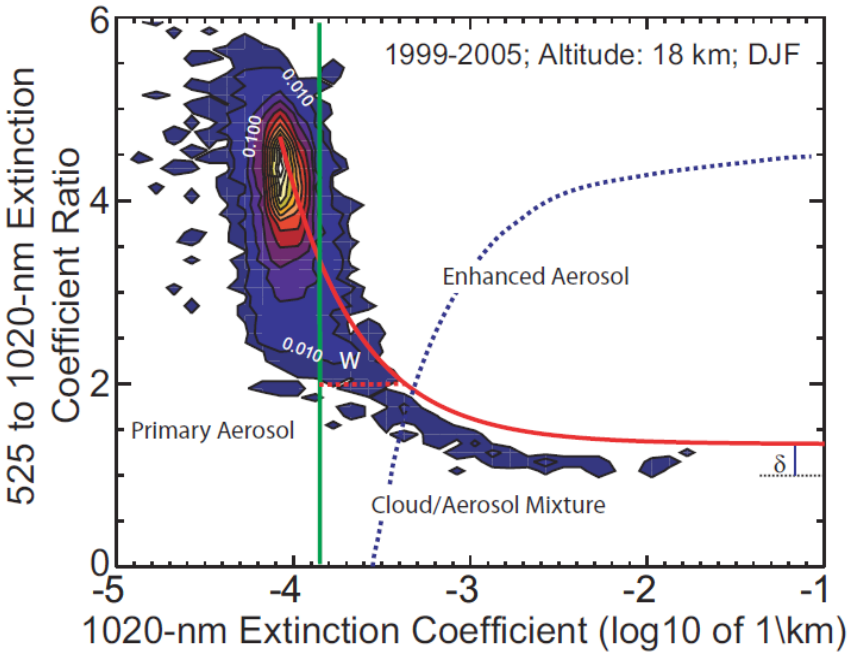

Figure 2.3: 18 km 1999-2005 DJF scattered data of SAGE II Extinction coefficient 525 nm and 1020 nm relationship presented with an aerosol centroid where peak data-density for extinction coefficient ratio above 2 is located, and *cloud centroid* located at ratio 1 at high 1020 nm extinction coefficients. Red line representing *R* from Eq. 6 together with the green boundary line illustrating cloud/aerosol separation method of Thomasson and Vernier (2013). The dotted blue line of *Enhanced Aerosol* represents the approximated Kent method classification line (Eq. 7), and the *W* represents the *wedge* region (later discussed). Figure is acquired from Thomasson and Vernier (2013).

3. Aim

The indirect main reason for this gross research project is to add knowledge to the highly uncertain stratospheric aerosols impact on earths radiation budget and its influence on climate change suggested by the IPCC climate models, and then made known to policy makers around the World.

1. I aim to observe and handle data from a satellite instruments such as SAGE II and SAGE III. It is desired to learn how the collection of data functions by the instrument and the satellite it inhabits. Including what functional implications a satellite instrument could have on the resulting formatted data I will present, including orbit, occultation etc.

2. A major portion of this project is dedicated to try creating a cloud algorithm that removes an acceptable amount of cloud interference in the extinction data to observe the stratospheric and upper tropospheric aerosol load between 1984 to 2005. Two papers with respective cloud masks have been selected to act as foundation to our cloud removal procedure and it is intended to find the best path using; Kent et al. (1993) with Thomasson & Vernier (2013) and Pitts et al. (2008). Additionally, latest existing datasets (Jul. 2017 to Sep. 2019) from SAGE III on ISS will be subjected to this cloud algorithm and its resulting extinction coefficients examined correspondingly.

3. For resulting data compilation, I aim to create an aerosol optical depth integration over certain layers of the atmosphere and over specific latitude bands after cloud removal. Additionally, I wish to produce a 525 nm and 521 nm AOD value with weighted means on the number of datapoints per latitude. Lastly, deciding on methodology to fill in values where there is missing data. With this lost data being the outcome of our cloud algorithm removing data or possibly other original interferences in the dataset mentioned above (2000 SAGE II malfunction). Choosing between acceptable methods of extrapolation and interpolation for extinction coefficients and the AOD I expect some variation in the results. These methods and results will be compared to presented values in Friberg et al. (2018) as well as GloSSAC (Thomasson et al. 2018) data for discussion.

4. Method and Application

4.1 Handling and Illustrating Data

The first task at hand was creating several applicable illustrations to interpret the extinction coefficient from provided SAGE II datasets in various spatial and temporal resolutions by generating suitable colorized figures and graphs. These figures will help to recognize cloud interferences and aerosol extinction at e.g. volcanic periods and contribute to creating a suitable cloud algorithm.

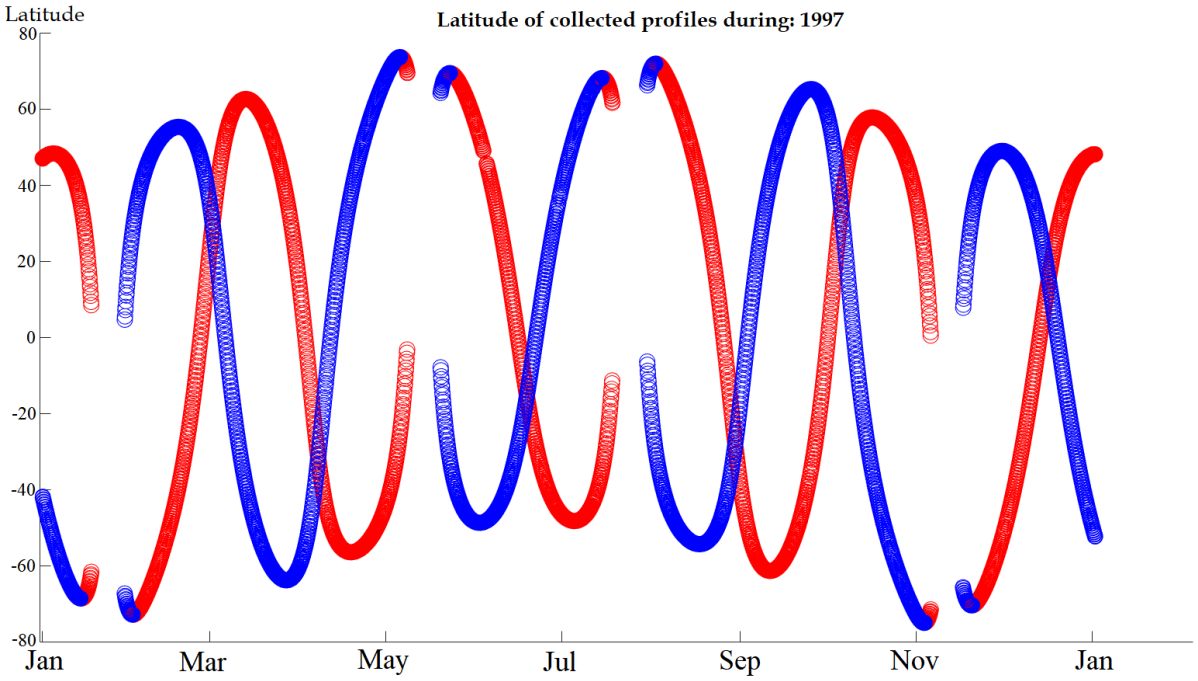

Figure 4.1: Example made from the data to observe how SAGE II collects one sunset (red) and one sunrise (blue) event with a vertical profile per orbit at two latitudes for the year 1997. The mentioned typical temporal gaps of missing data are seen in the figure as the latitudinal data coordinates are plotted against its specific day of the year it is collected.

Firstly, the data are plotted and studied in figures as vertical atmospheric profiles, this is how they originally are presented in the data matrixes, see Fig. 4.2. The data also included a dynamic tropopause seen in Fig. 4.2, and as stated before; all the mentioned *raw data* was (ahead of this project) generated from SAGE II algorithms (including corrected/adjusted through version 7.0, Damadeo et al., 2013). I assume that this static tropopause is reasonable for this study. In the data-handling it was recognized and mentioned in previous studies (M.P. McCormick, 1987) that the data is not spatially or temporally complete, as the provided data, based on a nearly 35-year-old satellite, had missing bands of latitude and sometimes missing whole months of non-collected vertical profiles. This could be partially explained by how the satellite collects data during its 57-degree inclined orbit in the sunrise and sunset events seen in the example in Fig. 4.1, with known instrument malfunction mentioned in Thomasson et al. (2008).

Contemplating Fig. 4.1 tells us there are latitude-bands with a significantly larger amount of vertical profiles included in the data for certain months, also latitudes exceeding ~80º north and south are virtually excluded by this satellite due to its inclination (McCormick et al. 1987). The vertical profile of Fig. 4.2 is an example of a clean UTLS profile where no signs of cloud signals above ~5km are shown. The 386 nm and 452 nm extinction are limited and considered untrustworthy and is given the dissipation seen in Fig. 4.2 for a large majority of data profiles, not reaching below 12–16 km due to molecular scattering from gases and ozone (Thomasson and Vernier 2013). These channels are not further investigated, and I am relying on recommendations by the previous studies not to include these wavelength bands when regarding the cloud algorithms. Full uncertainty analysis of the produced extinction coefficients, TP and modelled parameters are not included in this study but shown in figures for potential discussion.

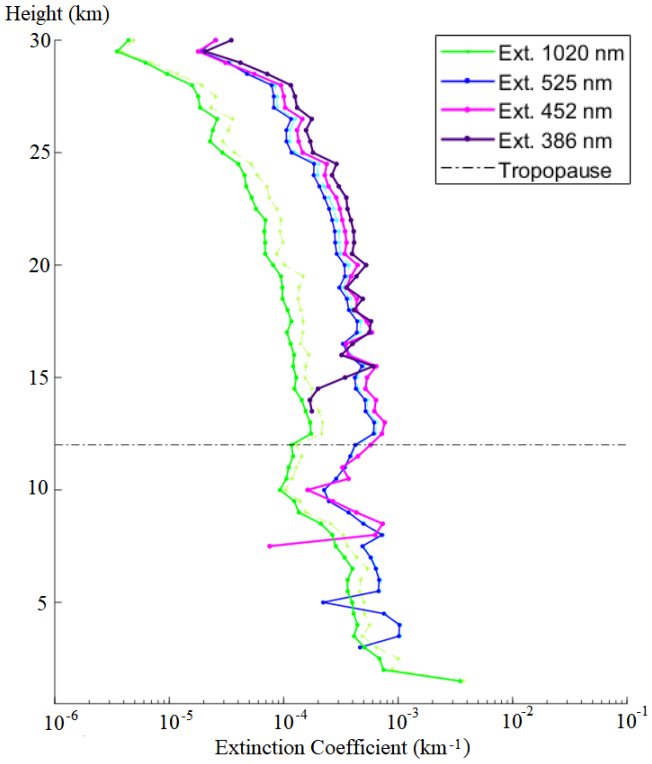

Figure 4.2: Example of one created vertical profile to represent coordinates 43°S 172°W of November 29th, 1998 including all extinction coefficient wavelength channels provided in the version 7.0 data on a logarithmic scale. Plotted percentage uncertainty (light-coloured dotted lines) are included for 525 nm and 1020 nm extinction coefficients. Here the 386 nm data does not include extinction below the TP and the 452 nm dissipates below 8km. 1020 nm extinction coefficient uncertainty exceed that of the 525 nm extinction coefficient in nearly all the data profiles.

4.2 Application of cloud algorithms to SAGE II

With the goal to provide the atmospheric aerosol extinction coefficient over our diverse vertical, temporal and latitudinal/longitudinal locations, I wished to create and implement a cloud mask based on previous studies on SAGE II data. With the purpose to free/smooth the data of cloud interference and show mainly aerosol signals. As mentioned above, I apply methods composed in Kent et al. (1987) and Thomasson and Vernier (2013), but with the knowledge that these papers are using older versions; 1.0 and 6.2 of the SAGE II datasets respectively and may differ. The changes include e.g. adjustments of the extinction coefficients from comparisons to other satellite datasets (Damadeo et al. 2013).

4.2.1 The 1993 method of cloud removal

The process of creating a suitable cloud mask for the SAGE II v7.0 data is principally reliant on an approach made by Kent et al. (1993), also referred to as the Kent method in this paper. Using the earlier mentioned relationship between the extinction coefficient of wavelength-channels 1020 nm and 525 nm I re-create the formula for classification of cloud, and non-cloud products from Kent et al. (1993).

Regarding the applied Kent method seen in Fig. 4.3c-d, observe that the intersect on the x-axis is located much closer to zero using this method and likely classifying our data inaccurately. This could be due to the difference in our version of the data as the σ- value represented in Kent et al (1993) could be much higher when re-creating the exact example of datasets (temporally and spatially), and potentially resulting that their

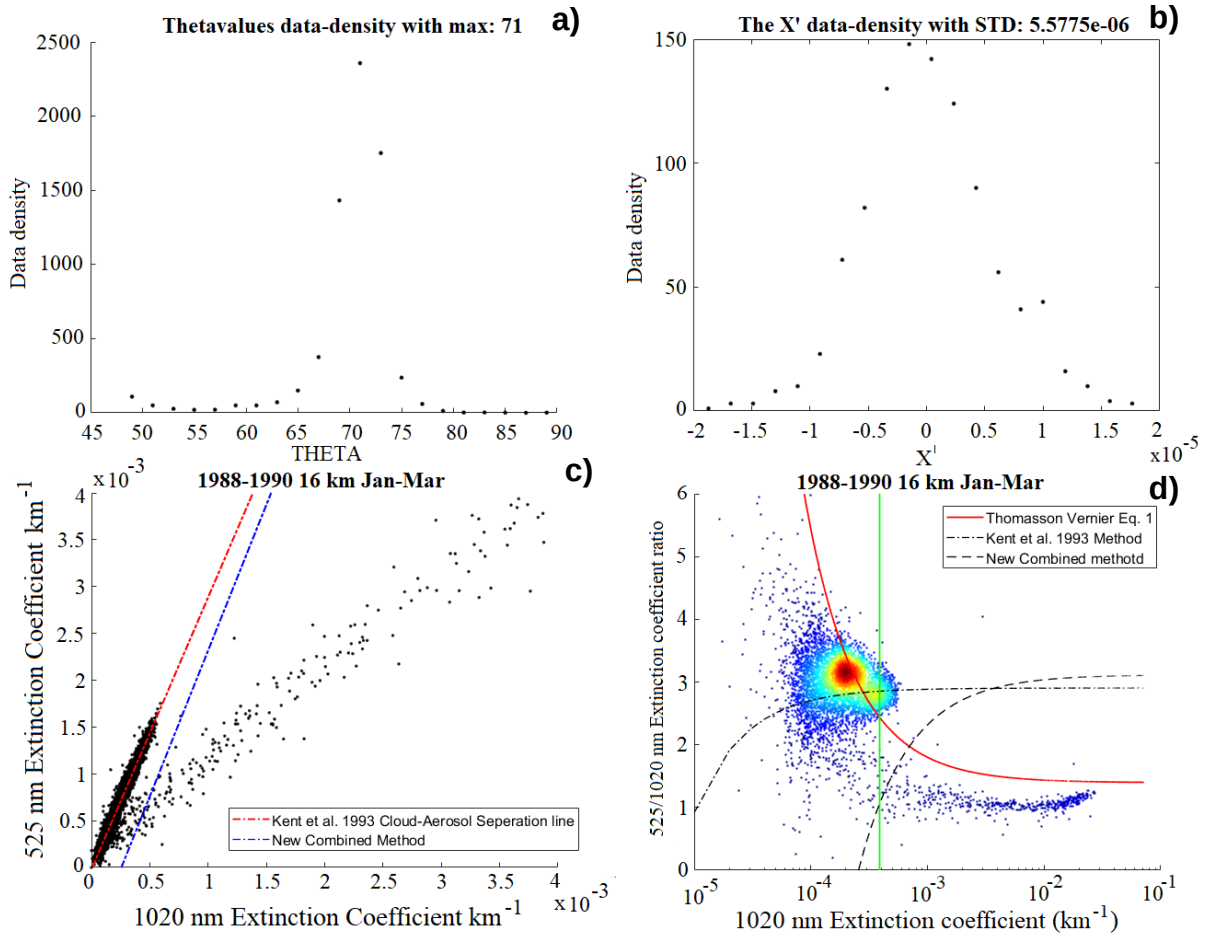

Figure 4.3: 1988–1990, JFM of 16 km, re-created example using Kent et al. (1993) **a)** with θ-data density from an angle to find in what angle (θ') most number of data-points are located in the plot, **b)** taking the datapoints contained in θ' and calculating the standard deviation (σ seen in **b**) from a normal distribution **c)** resulting classification line from Eq. 5 method shown in **a-b** (Kent et al. 1993) and our new combined method (blue line, Eq. 8) using a differently defined value for intercept on the x-axis (described in section 4.3). **d)** Result illustrating same values as **c** but in a plot using a y-axis in a ratio as in Thomasson and Vernier (2013) Fig. 2.3, with all three methods of cloud/aerosol classification is seen including our new combined method.

v1.0 data includes higher deviations in the extinction coefficient data compared to our v.7.0 computed dataset. This could explain why the $X_0' + 2\sigma$ is too small in these cases for Eq. 5. I focused on the latter Kent version method for creating the combined method described in the next section.

4.2.2 The 2013 method of cloud removal

Differences in time-period of interest from Thomasson and Vernier (2013) was considered when comparing application of their method of cloud/aerosol classification to our results. Kent et al. (1993) uses latitudinal separation for the data when applying the cloud algorithm, e.g. from 40-60º, while T.V. and our method include all latitudes for a 3-month period on each of the 0.5 km vertical resolution levels (see example *fig.4.3d*). The Kent method with latitudinal categories may be more valid as e.g. 12 km in the tropics could be considered a tropospheric airmass while it is a stratospheric airmass on higher latitudes. However, the limitation of data from SAGE II that the T.V. method has from 2000-2005 (least half the datapoints missing from instrument malfunction) compared to Kent method data early in the SAGE II operational lifetime (1985-1991) probably forced Thomasson and Vernier (2013) to include all latitudes As insufficiently when large aerosol cloud signals are included in the vertical profiles. However, volcanic aerosols are inhabiting the atmosphere considerably during the SAGE II lifetime. An example, and a potential limitation, when applying the T.V. method

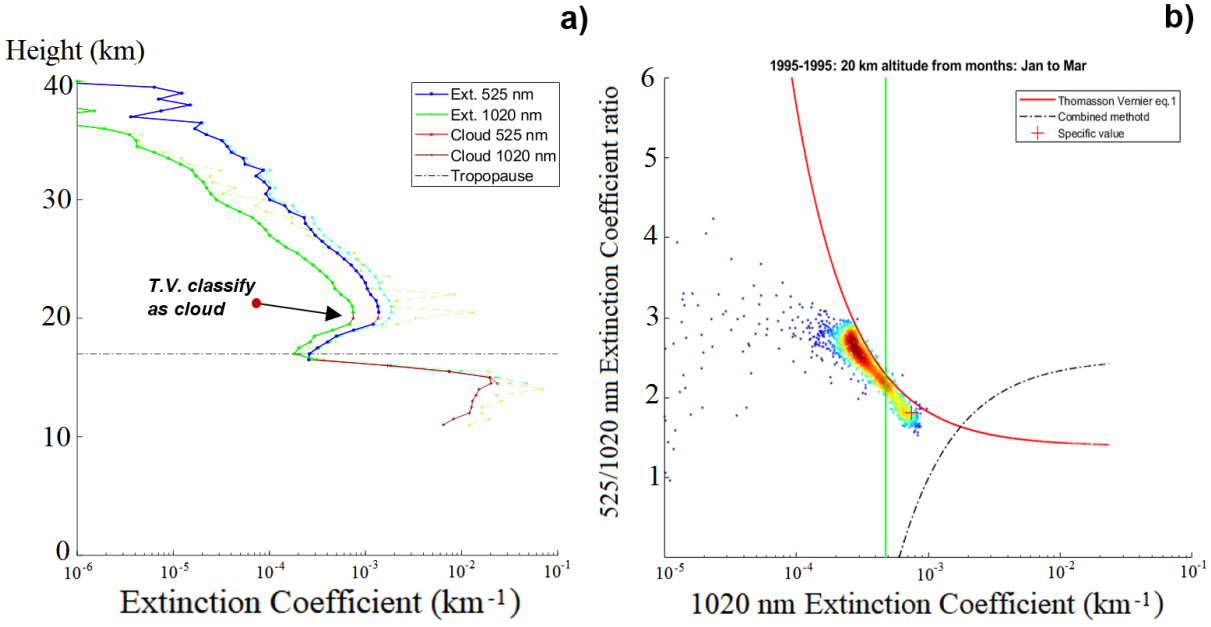

Figure 4.4: Example of **a)** a vertical profile with T.V. method cloud removal seen in red for 2°N and 160°E, 13th of May 1995, with C-Ext (in legend) representing cloud-classified values of Extinction coefficients **b)** 20 km, January-March scatterplot and the cloud classification equations with the dotted circled red point in **a** plotted as a red cross, showing that the T.V. (2013) method of cloud removal possibly inaccurately classifying aerosols signatures. However, these post-volcanic periods show high stratospheric aerosol loads and are not included in the Thomasson and Vernier's study period of ATAL but are included in my period.

on a volcanic period is seen in Fig. 4.4 following four years after the eruption of Mt. Pinatubo (still high stratospheric aerosol load). The dispersion of 1020 nm extinction coefficient values for the aerosols centroid during this period is larger than T.V potentially accounted for and the method of using absolute median deviation k_a + 3Δk_a (see green line in Fig. 4.4) gives that the factor 3 is insufficient (too small) in this case. They will categorize these volcanic aerosols as clouds occurring at 20 km, which are not considered to be accurate by our evaluation of aerosol vs cloud extinction signature.

4.3 New combined method

Before considering creating a new method for cloud/aerosol classification, I initially applied the method by Thomasson and Vernier (2013) and their interpretation of the Kent method on the v.7.0 data to investigate the performance of these two on the entire dataset of SAGE II from 1984–2005. Some examples are described and seen in Fig. 4.3 and Fig. 4.4 which includes sequences where I are not satisfied with their methods based of examples I will give in the following sections. Fig. 5.1 include results of how I observed a potentially inaccurate classification at 20 km in a monthly mean plot also seen in Fig. 4.4.

By carefully selecting years in which to jointly perform the cloud algorithm, I got different responses for the cloud algorithm as seen in Fig. 4.5 and the bottom row (Fig. 4.5c-d*)* showing a more uniform aerosol centroid, which are chosen for the new main cloud mask in this case. These centroid appearances are shown mostly following the volcanic events and these years are more separated when applying the cloud mask for this explained reason, see selected years in Table A1. The volcanic residue during these periods show expected higher extinction coefficients values, this could be connected to a higher particle size distribution of aerosols in the stratosphere from an eruption. This is what the secondary centroid is a potential result of in Fig. 4.5a. For SAGE III, each year had to be run through the algorithm separately as there is higher volcanic and forest fire activity seen compared to SAGE II. The aerosol centroid 2017-2019 changes in characteristics drastically each monthly plot, see Fig 5.3 for examples.

The method suggested by Thomasson and Vernier (2013) on moving the line of 1020 nm x-axis intersection (k_a + 3Δk_a) by varying the factor *3* in the equation with respect to heights (below 12 km) was used in our *new combined method* seen in Fig. 4.5. However, T.V. settled on an *empirically robust* value of the factor 3 for the green separation line. I implemented and revised this varying factor in our Eq. 8 for the cloud-algorithm as large variations were observed in the mentioned absolute-median deviation for the aerosol centroid (525/1020 nm Ext coefficient ratio ≥ 2) when going above 18 km. Two values for the factor (k_{fac}) was chosen for our new combined method Eq. 8 that accounted for the volcanic change in extinction coefficients seen in Fig. 4.4.

$$\mathrm{R} = \mathrm{k_a} - \frac{(\mathrm{k_a} + \mathrm{k_{fac}}\Delta\mathrm{k_a}) * \mathrm{k_i}}{\mathrm{k}} \qquad (8)$$

As after applying the new Eq. 8 in various cloud classification scatterplots (seen in Fig. 4.4b and Fig 4.5), I concluded that it was enough to set; heights < 18 km: $\mathrm{k_{fac}} = 1$ and

for heights ≥ 18 km: $k_{fac} = 5$. Where exclusion seen in Fig. 4.4 was the major cause of an unsatisfying curve at high altitudes (above ~18 km) cutting into the aerosol centroid. Fig. 4.4 shows our new combined method (Eq. 8, dotted black curve) with initial value on the logarithmic x-axis higher than the green T.V. line as a result. In Fig. 4.5 we see the opposite, the dotted black curve now starts left of the green line for the 17 km plot, also with a classification that does not exclude large portions of the potential background aerosol extinction coefficient. More examples seen in the SAGE III data implementation of our new combined cloud mask in Section 5.2.

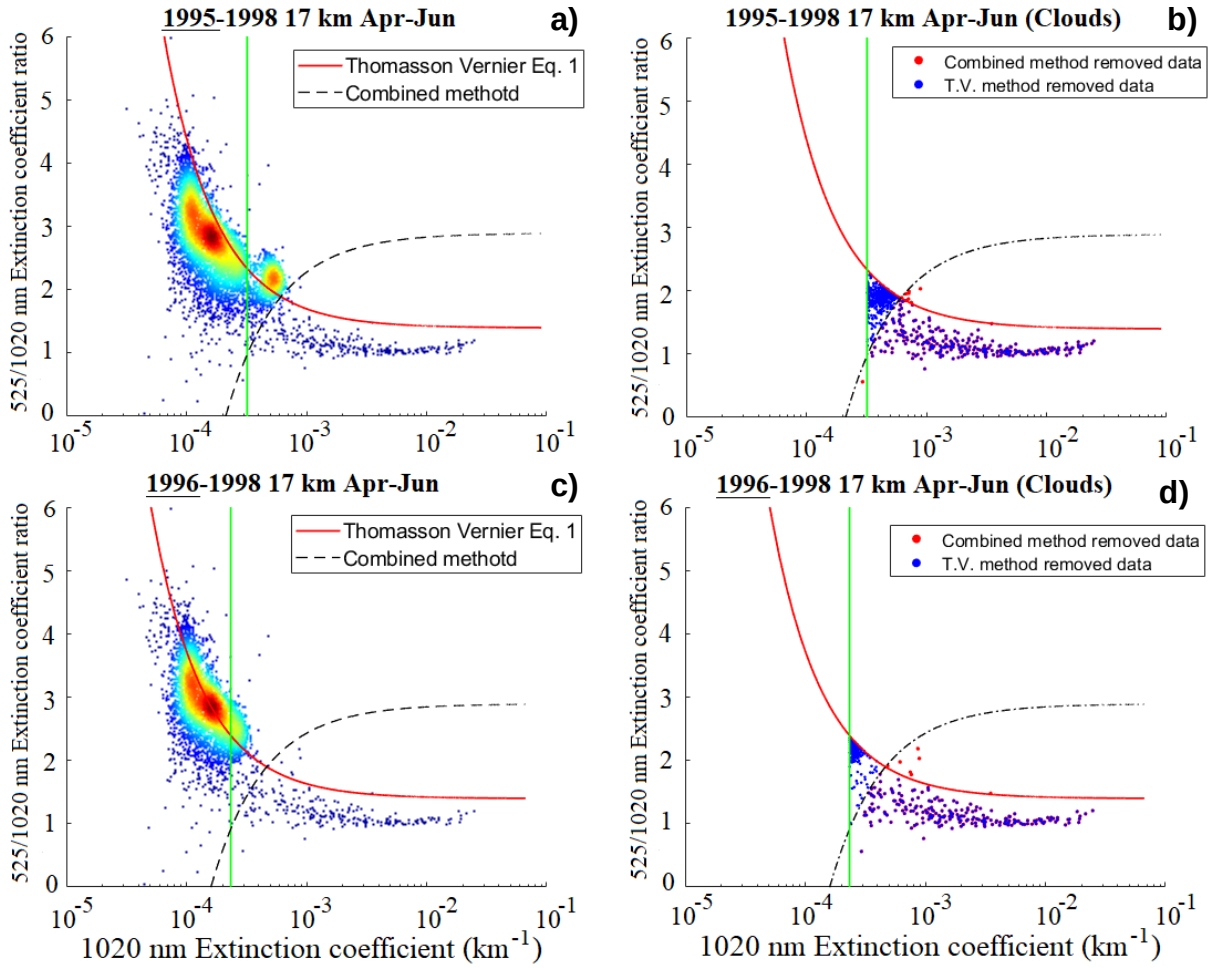

Figure 4.5: Example performing the classification scatter plot for all profiles at 17 km spanning April-June, plotted from years: **a)** 1995–1998, **b)** here with data classified as clouds and removed according to the two classification functions (*New combined: red,* and *T.V: blue).* **c)** Applied new period of 1996–1998 with smaller centroid of (volcanic) aerosol, **d)** same as **b** but for plot: **c**.

Cloud mask application on months July 1991 to December 1993 closely following Pinatubo, was excluded due the bulk of missing data during this period. The cut-off for values in the data exceeding the threshold for extinction coefficients during this period made by the SAGE instrument algorithm gives us too few values to include in a potential cloud algorithm for this period, see monthly representation examples in Fig. A2.

4.4 Method for polar stratospheric clouds

Some techniques for eliminating polar stratospheric clouds in our cloud algorithm have been tested and compared with previous methods to identify and filter out PSC's for SAGE occultation data. Thomasson and Vernier (2013) and the GloSSAC project make some effort in trying to remove these clouds. Testing their methodology and using a compilation of specific altitudes, latitudes and their 195 Kelvin threshold temperature based of the study by Pitts et al. (2009), I observed some elimination of potential PSC data (see Fig. 5.2). However, interference I hypothesised to be caused by the onion peeling method by the SAGE II data-model, creates a discrete spatial distribution of possible PSC signal in the monthly-mean plots (see Fig. 5.2). Pursuing this appearance with a detailed investigation on the specific region where I detected high extinction coefficients in polar stratospheric data, I constructed a new method of elimination, see Fig. 4.6. Using Eq. 6, I empirically constructed new δ and k_a values (Table A.1) to the equation (see PSC separation line in Fig. 4.6), carefully chosen for each time-period and height, as I did for our previous *new combined* cloud method, see *PSC separation line* in Fig. 4.6. The separation line is constructed to cut between the two centroids without removing much of the background aerosol signatures (left lower extinction coefficient centroid).

The method of identifying PSC through a temperature threshold, used by Thomasson and Vernier (2013), is constructed for CALIPSO lidar instrument data, and do not have to consider the onion peeling like in the SAGE algorithm. Pitts et al. (2008) suggests that PSC can be observed between ~8 and 30 km altitude and I observe modelled temperatures below 200 Kelvin when we get high enough (≥14 km) in the atmosphere for a considerable amount of datapoints. This would classify values which would generally be classified as *background* aerosol extinction coefficients characteristics, see green, cyan and blue coloured datapoints in background aerosol centroid in Fig. 4.6. See Fig. 5.2 for resulting monthly mean of October 1999.

Worth noting that the SAGE II orbital limits the months of possible observation of PSC to mainly August to December, as latitudes south of 60°S are predominantly not captured in the SH early winter season, especially after the SAGE II malfunction in 2000. The method performance seen in Fig. 4.6 and Fig. 5.2 was compiled using multiple of these image-comparisons. Here I had to weigh the amount of potential removed data against filling gaps through inter/extrapolation (see next section), as removing too much aerosol signature would present our results with a potential underestimation. After both cloud-types were classified and eliminated I still observed many datapoints remaining locally surrounding the eliminated cloud-data in the vertical profiles. This could be related to the cloud interference to the SAGE onion-peeling method mentioned above (see Fig. 2.1). I chose to eliminate the 0.5 km over and underlying vertical extinction coefficient value in effort to remove this interference. The results from this method is seen in the model results for Fig. 5.1 between the T.V. method and ours, removing additional individual pixels with high extinction coefficients located above a removed cloud-pixel.

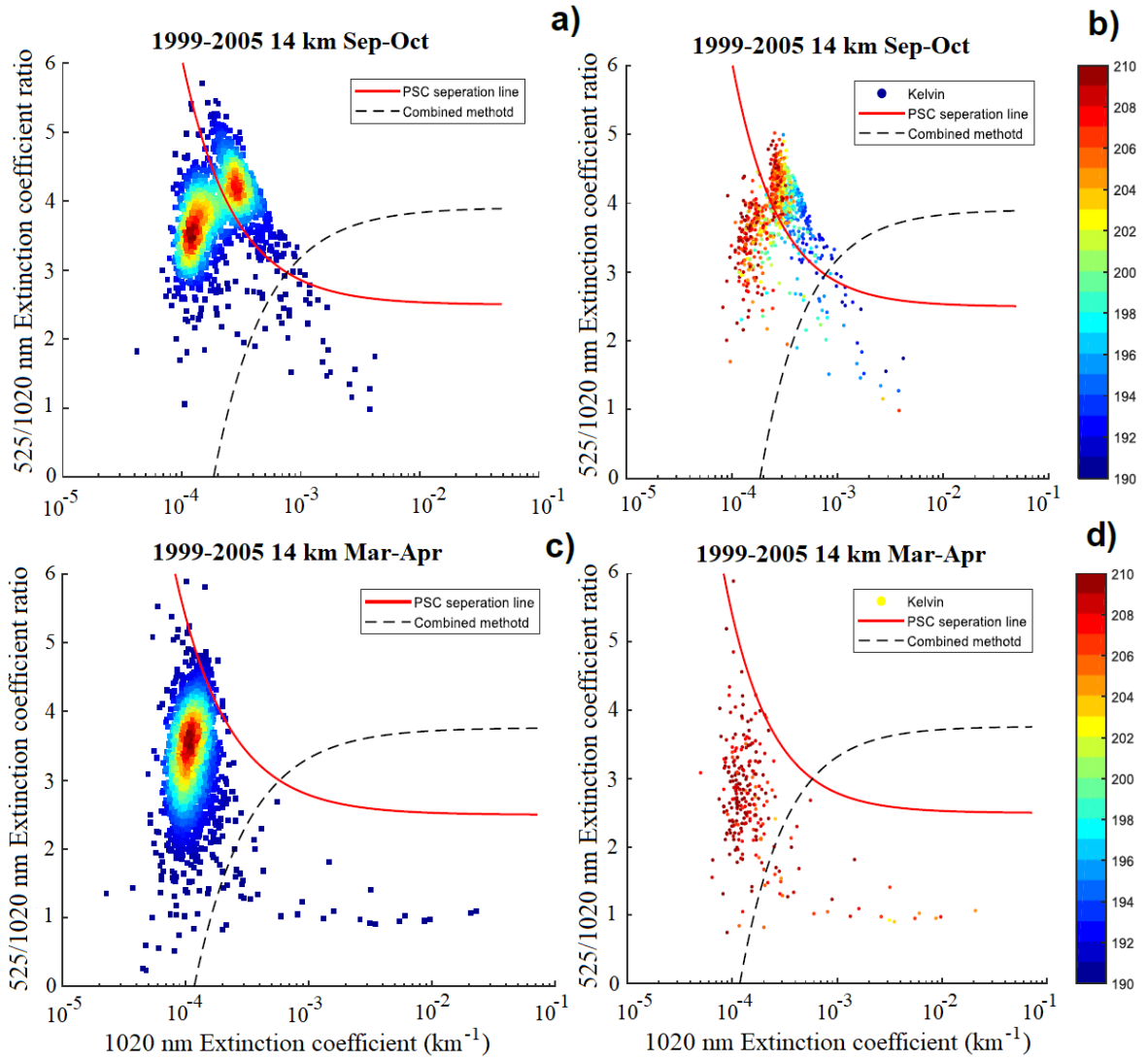

Figure 4.6: Example performing the new PSC classification scatter plot for all profiles at 14 km within years 1999–2005 and **a)** September to October 60–90°S with data density as colour scheme. **b)** Here replacing colour scheme in **a** with modelled temperature in Kelvin, **c)** same as **a** but for PSC-free months March to April (Autumn) **d)** same as **b** but for plot **c**.

4.5 Data extrapolation and interpolation

After running the cloud algorithm over our extinction coefficient data of the 1020 and 525 nm channels I was left with empty values in our stratospheric data near the TP and where PSC are removed. To create the AOD curves and illustrate figures representing the SAGE II and SAGE III observations adequately I settled to fill these empty datapoints with the nearest value (vertically) in the stratosphere and down to the TP. This method is corresponding to Thomasson et al. (2018) where the GloSSAC data sets used a similar extrapolation method for their SAGE II cloud algorithm (the T.V method). The alternative methods of applying linear and polynomial extrapolation and interpolation of stratospheric data down to the TP and surrounding PSC could in some cases yield a more uniform profile of the extinction coefficient. But these methods

resulted in some cases with extreme decreases and increases due to our 0.5 km layers varying occasionally in extinction coefficients values by factors over 5 per vertical step. Example of our prudent inter-extrapolation technique used to fill cloud-pixels seen in Fig. 4.7.

Following the new datasets after cloud mask application and the removal of extinction coefficient-values classified as clouds or PSC was complete, I was left with new vertical profiles to compile. Using Eq. 2 I sought to create a global latitude weighted mean AOD curve in relevance to Friberg et al. (2018) and previous studies in the GloSSAC project (Thomasson et al., 2018) divided into sections of the atmosphere, see Fig. 5.5. A temporal linear interpolation is performed on our LMS, 380–470 K, and 470K–40 km regions with the 1° zonal monthly mean AOD between 60°S to 60°N. However, an exception for the missing tropical data in June 1991 was necessary due to the drastic change in aerosol load from June to July caused by the mt. Pinatubo eruption, see top image in Fig. 5.4. GloSSAC (Thomasson et al. 2018) elaborated on various interpolation methods for this month but agreed on using tropical values in May 1991 to fill the missing data in of June, and I chose the corresponding method for our AOD interpolation for later comparison. This is could however potentially underestimate the AOD of days in June following the main eruption that occurred on June 15th (Thomasson et al 2018). See our steps of inter and extrapolation in Fig. 5.3.

The extrapolation, seen in bottom image of Fig. 5.3, to fill high-latitude values from 60° to 80° north and south, is executed through a latitude mean of the closest 5 existing latitude values in the same isentropic layer (LMS, 380–470 K, and 470K–40 km). Thomasson et al. (2018) elaborates on a similar method using an *equivalent latitude* of a temporal mean with respect to the polar vortex and secondary observations by MERRA. However, I decided on our simplified method based on the estimation that the isentropic layers prove homogeneously enough in its to spatially extrapolate the AOD to higher latitudes.

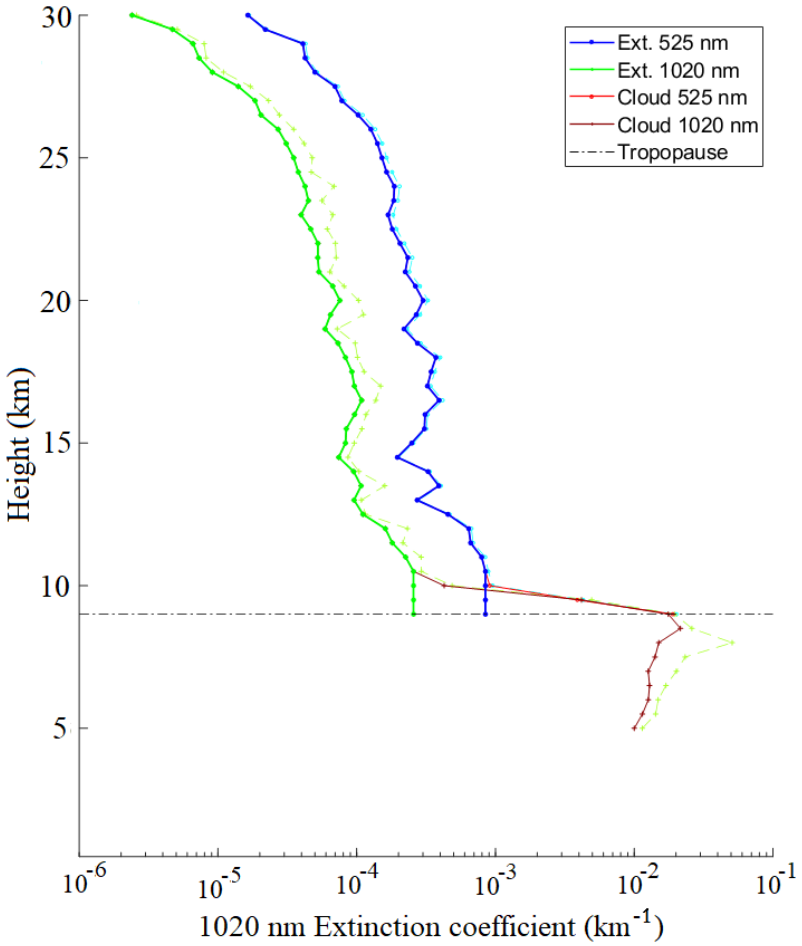

Figure 4.7: Example of one vertical extinction coefficient (km^{-1}) profile of February 5th 1999, 53°S and 157°W with plotted uncertainty (light-coloured dotted lines) on a logarithmic x-axis. Red values represent where our classified cloud data have been removed and then filled through extrapolation down to the tropopause (the blue and green line 9.5-11 km).

5. Results

5.1 Cloud mask performance on SAGE II

Fig. 5.1 show example of less removed datapoints (black spots) for the new combined method in the stratosphere compared to the T.V. method (middle image). Additionally, Fig 5.1 show examples of where higher abundance for single tropical extinction coefficient data-values ($\geq 3.5 * 10^{-3}$ km^{-1}) are remaining in the UTLS for the T.V. method image (8°N in 1995 and 6°S in 1996). Both methods removes a large majority of the high cloud signatures compared to the raw data image (top row Fig 5.1), with the mentioned *Sulphuric Aerosol Layer* still visible over the ~17–20 km stratospheric region. With higher extinction in 1995 than 1996 from sulphuric residue

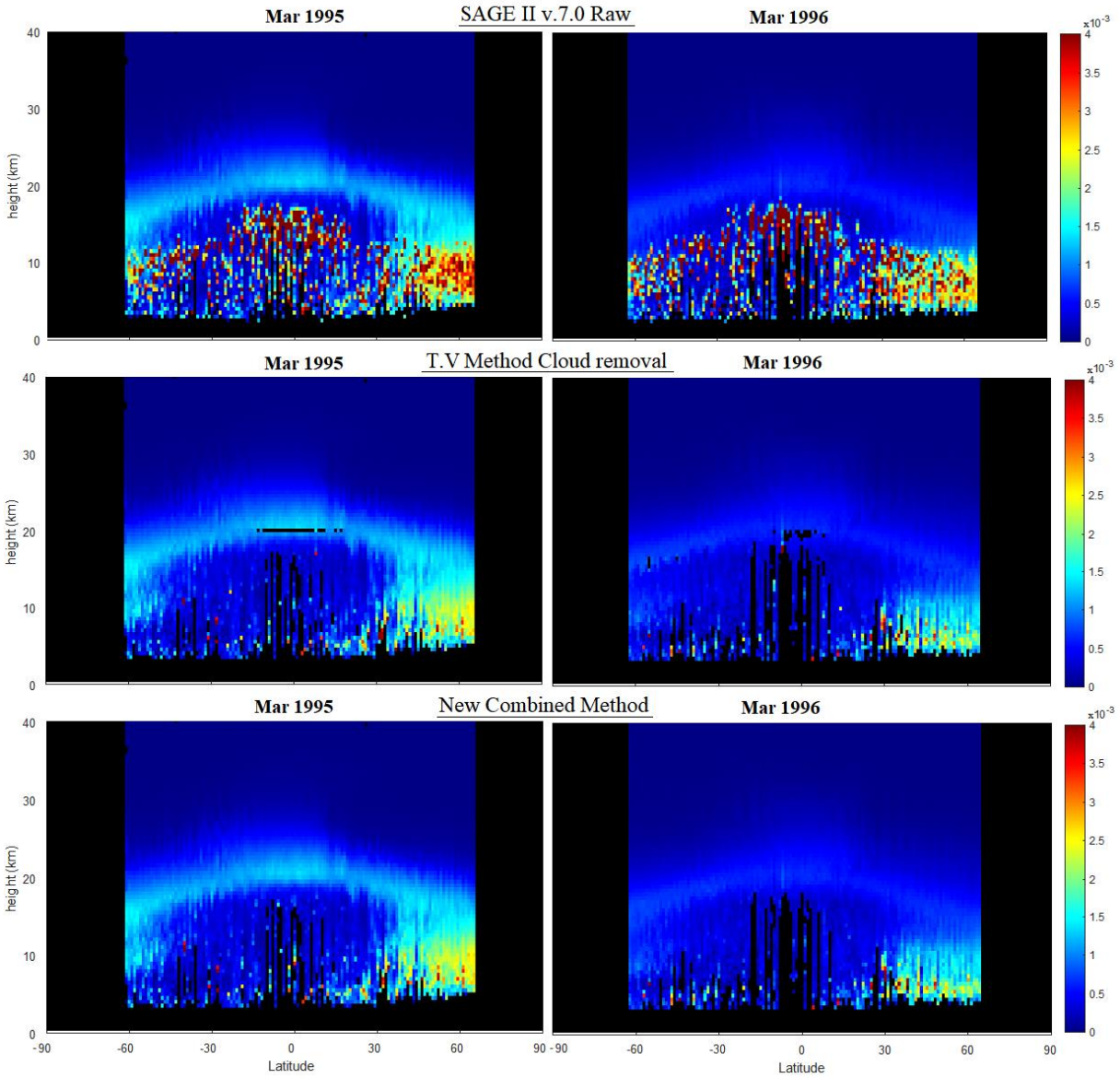

Figure 5.1: Example showing the monthly mean 525 nm extinction coefficient (km^{-1}) in a colour-scheme for March 1995 and 1996, plotted Original SAGE II v.7.0 (with no cloud mask), and the applied T.V. (2013) method cloud mask, with bottom row figures representing applied new combined method cloud mask.

from mt. Pinatubo 1991 as expected. Note a high tropospheric and UTLS 521 nm extinction coefficient in the NH mid-latitudes with aerosol signature for Fig. 5.1, again higher for 1995 than for 1996.

For Fig. 5.2, observe the elevated extinction coefficient in the southern hemisphere TP–16 km region potentially related to PSC. The figure shows how the T.V. method of PSC classification (Fig. 5.2 middle image) clears a portion of the potential PSC-signature but parts of the elevated stratospheric extinction coefficient region is still clearly present. Our new method of classification separating the two centroids (seen in Fig. 4.6) yields a more uniform polar stratospheric appearance (right image Fig. 5.2) for all cases of observed potential PSC signature in the monthly mean data-images.

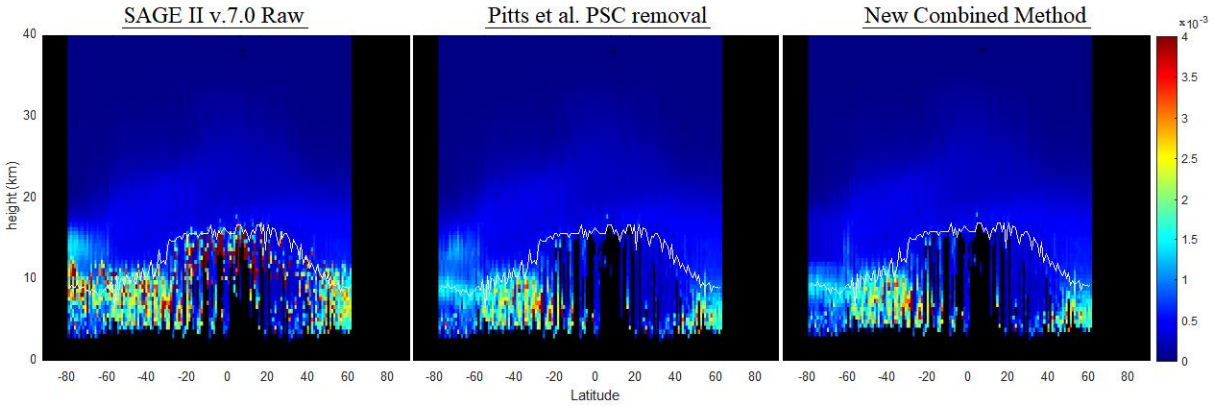

Figure 5.2: Example showing the monthly mean 525 nm extinction coefficient (km^{-1}) in a colour-scheme for October 1999, plotted Original SAGE II v.7.0 (with no cloud mask), and middle image show our mask for cloud-removal added with the applied T.V. thermal method for PSC mask based on Pitts et al. (2009), and right image show our mask for cloud removal applied with the new PSC centroid-based mask. Zonal mean tropopause height is plotted as a white line.

5.2 Cloud mask performance on SAGE III

One volcanic event with elevated stratospheric extinction coefficients for SAGE III is observed in August of 2018 in Fig. 5.3a-b and Fig. 5.6. The branched aerosol centroid of Fig.5.3a-b is potentially caused by this high volcanic extinction mentioned earlier (the two centroids in Fig. 4.5a). Note that Fig. 5.3a is 6 months after the eruption and may show this appearance as the volcanic aerosols travelled poleward (more in the SH) in the lower branch Brewer-Dobson circulation (380-470K layer). The meridional gaps of large extinction coefficient values observed near the point of eruption, seen in Fig. 5.3b and Fig. A2, is caused by large longitudinal and temporal variations in the monthly mean data (example; Fig. 4.1). The effect of elevated extinction coefficient from potential PSCs at ~60°S in Fig. 5.3a is noted, but not further investigated.

Fig. 5.3c show a special case where the known extreme 2017 August wildfires in the Canadian province of British Columbia (50°N) ejected large amounts of aerosols reaching into the stratosphere (Khaykin, 2018)**.** This could explain the signal seen in

Fig. 5.3c and the appearance of a secondary cloud-tail in the scatterplot, where most of this signal is removed in our cloud algorithm (values under black dotted line). No wildfire signal have been accounted for in our study for the SAGE II dataset and our mask is thereby negligent to this appearance for now.

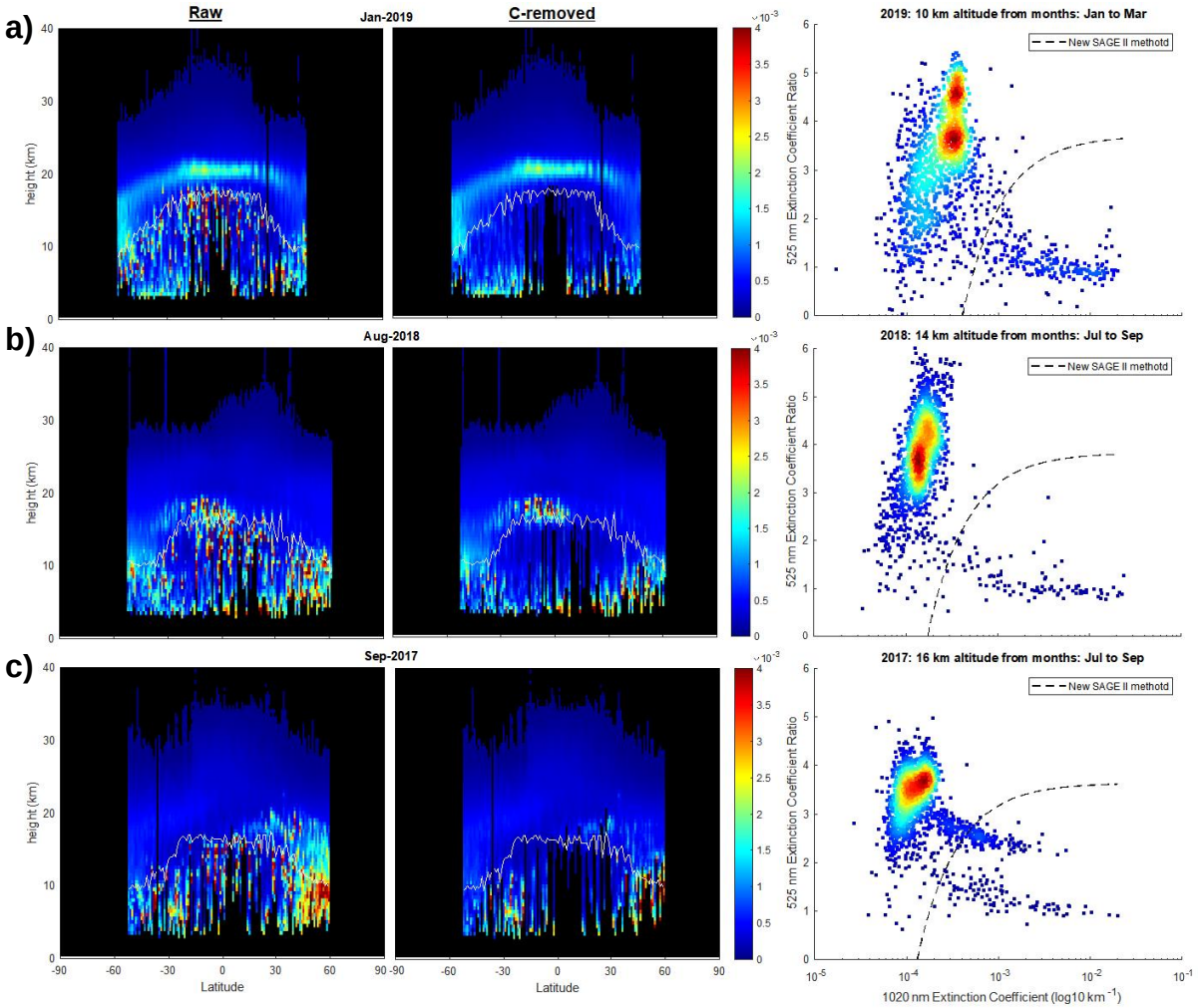

Figure 5.3: Example showing the SAGE III resulting raw and cloud-free monthly mean 521 nm extinction coefficient (km^{-1}) in a colour-scheme with respective density scatterplot (right column) of cloud classification for **a)** Jan 2019 and 10 km Jan-Mar, **b)** Aug 2018 and 14 km Jul-Sep, **c)** Sep 2017 and 16 km Jul-Sep.

5.3 Aerosol Optical Depth

The volcanic eruption events that indicate stratospheric signatures in Fig. 5.4–5.6 showed greatest initial presence on the hemisphere where it is located, exception for the extreme Pinatubo event. The remains of the heavy El Chichón eruption (17°N) in 1982, has already distributed its stratospheric aerosol equally to both hemisphere before start of SAGE II (October 1994), which causes the initial high value in Fig 5.4 and Fig. 5.5 of elevated AOD over 10^{-2}. For Pinatubo, with the massive AOD signal (10^{-1}), observe a relative equal distribution between the hemispheres almost instantaneously due to its immense magnitude but with a slight peak on the northern hemisphere. The smaller eruption signals show similar distribution effects however

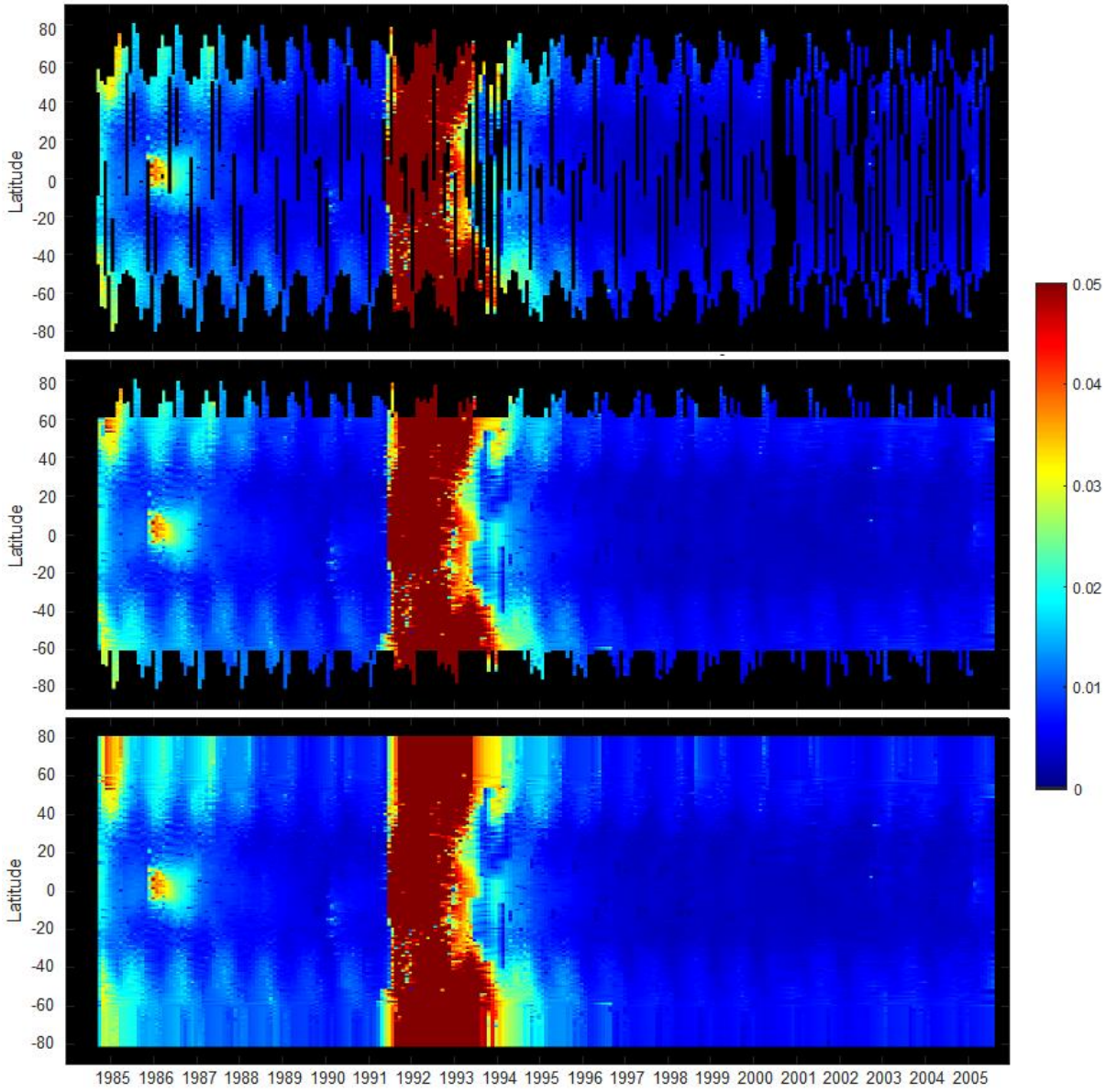

Figure 5.4 The resulting cloud-removed SAGE II total stratospheric (TP–35km) monthly zonal mean 525 nm AOD through last two steps of interpolation (middle image) and extrapolation (bottom image). The total stratospheric AOD was calculated through addition of the layers form Fig. A1; LMS, 380K–470K and 470K–35 km after they are individually inter/extrapolated.

they are less distinct. This was also heavily dependent on the atmospheric dynamics at the event latitude, as vertical and meridional transport changes between the tropics, subtropics, midlatitudes and poleward. These dynamics will be further mentioned in the next section.

A clear seasonality is distinct for Fig. 5.4–5.5 that influences the AOD magnitude of potential eruption signals, but likewise also alters in response to volcanic periods. The SH AOD is mostly elevated following ~June and NH AOD in winter following ~November. LMS show distinct greatest seasonal variability and the remaining two layers have more stable AOD but still noticeable seasonal fluctuations. This is additionally mentioned in the next section. In Fig. 5.6 the two eruptions referred to in the *Global Volcanism Program* (2013) are by mt. Krakatau (Indonesia) 6°S August 2018 and Sarychev (Russia) 48°N August 2019. The strong NH extinction signal seen in Fig. 5.6 may be related to the long boreal wildfire in Canada ~50°N mentioned above (Khaykin, 2018).

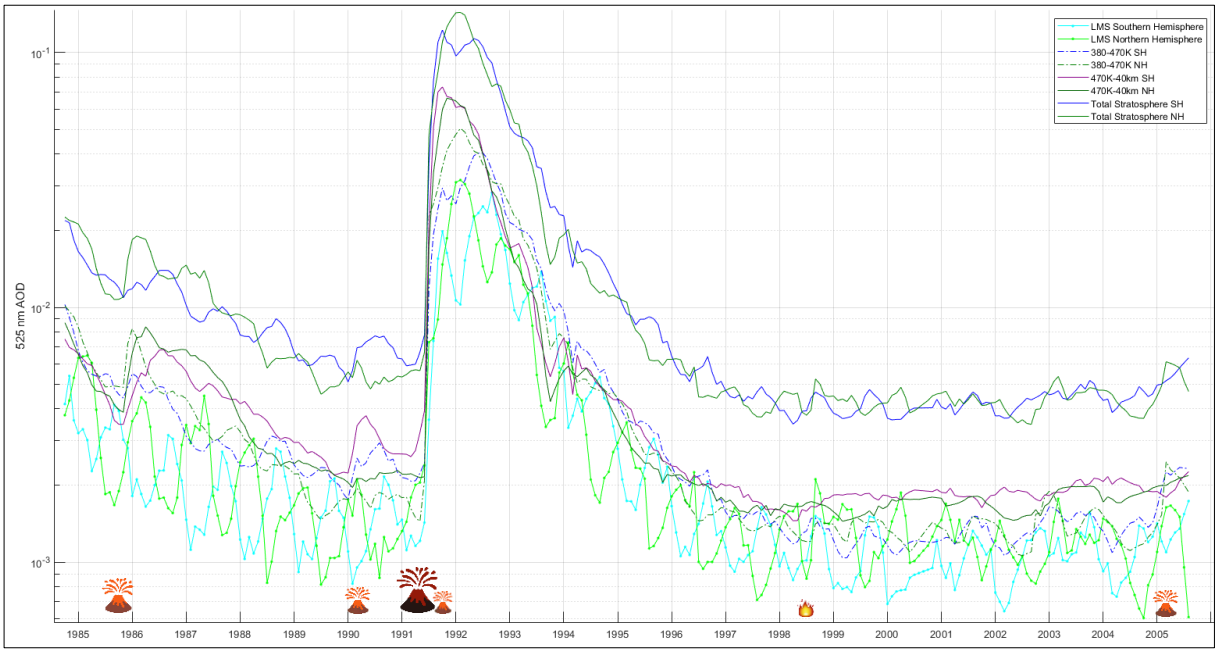

Figure 5.5 The resulting cloud-removed SAGE II stratospheric latitude-weighted mean 525 nm AOD on a logarithmic scale. Each line represents NH (greens) or SH (blues) of the total stratospheric AOD in the LMS, 380K - 470K and 470K - 35km layers. Large volcanic stratosphere signatures are marked at month of eruption (magnitude affiliated with size of figure) based of the *Global Volcanism Program* (2013). Chronologically; mt. Ruiz Nov 1985 (5°N), Kelut Feb 1990 (8°S), Pinatubo Jun 1991 (15°N), Cerro Hudson Aug 1991 (46°N) and Manam (4°S) 2005. Forest fire 1998 from Fromm et al. (2000).

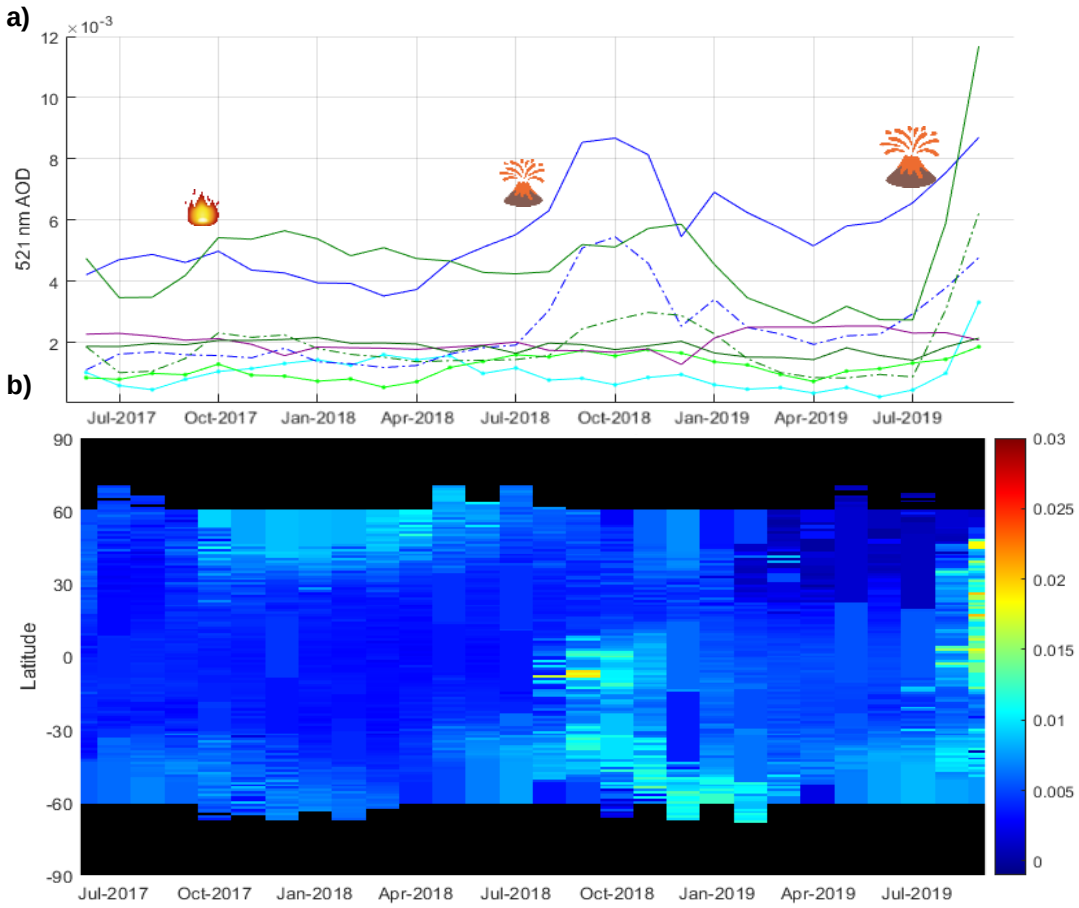

Figure 5.6 The resulting cloud-removed ISS based SAGE III **a)** continuing from Fig. 5.5, stratospheric latitude-weighted global monthly mean 521 nm AOD. Each line represents NH (greens) or SH (blues) of the total stratospheric AOD, 380K– 470K and 470K–40 km layers. Large volcanic stratosphere signatures are marked at month of eruption including the forest fire in 2017, see legend for Fig. 5.5. **b)** Zonal monthly mean total stratospheric 521 nm AOD (interpolated 60°S–60°N), note colour-scheme scale decreased from Fig. 5.4.

For Fig. 5.7, distinguish an agreement with the compared dataset of AOD, with a few cases of AOD differences between ours and GloSSAC's result. The most prominent is the Pinatubo event. This is where the GloSSAC dataset include a combination of CLEAS and HALOE on the SAGE II data following the eruption 1991-1994. Our mentioned brute extrapolation of missing Pinatubo data (Fig. A2) down to the tropopause is expected to yield potentially higher global AOD compared to their method of data assimilation after the eruption and is therefore suspected to cause this difference. The earlier drop in AOD for our data after ~1993 is also believed to be due to our means of inter/extrapolation. The cause of the GloSSAC peak for November 1984 in Fig. 5.7 is unknown, but I suspect some error in downloaded data from the ground and air-based lidar assimilation in our/their compilation code. Two remaining peaks of difference is seen for the 1998 wildfire and Kelut eruption.

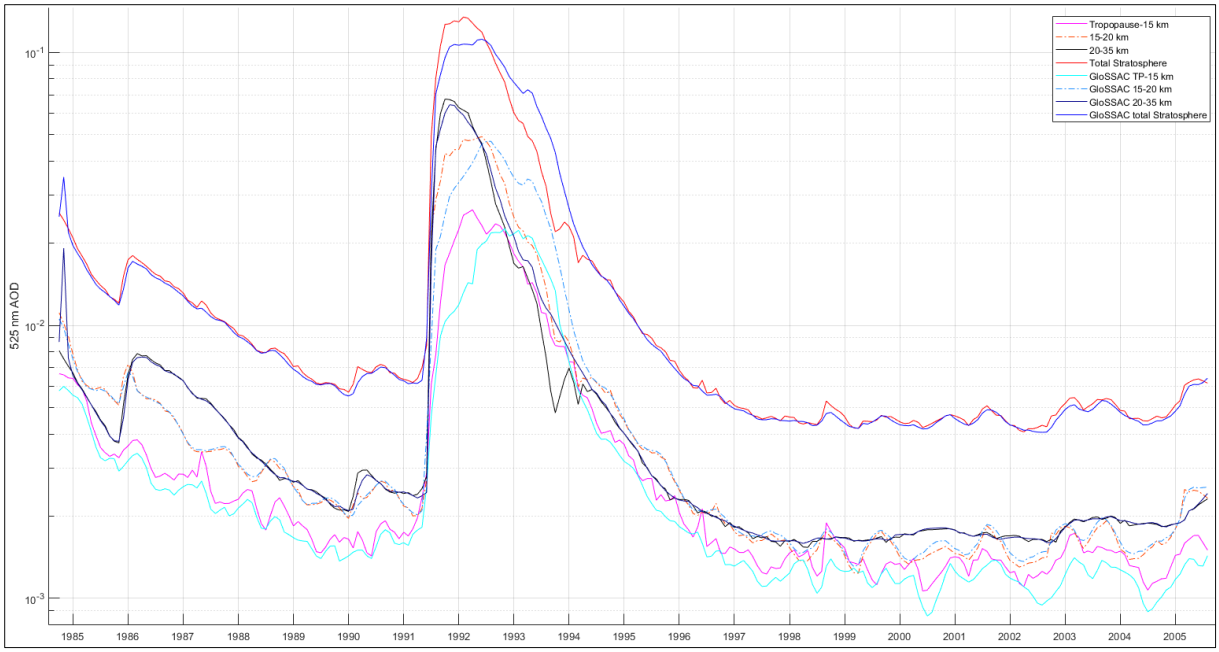

Figure 5.7 The SAGE II global (mean of Fig. 5.4) stratospheric latitude-weighted mean 525 nm AOD on a logarithmic scale with height-based layers from our dataset (reds) versus constructed SAGE II, CLAES and HALOE (SAM II with ground and air-based lidar for ≥1994) datasets (blues) from the GloSSAC project (Thomasson et al. 2018). See legend for data-colour specification.

6. Discussion

Some topics of discussion have been previously specified in our methodology and application together with our result section, and this section will elaborate on some parts of those mentioned subjects together with additional arguments.

The direction of our cloud classification methodology was, as mentioned above, a result of testing applications from previous methods and analysing the corresponding plotted figure result. I can state that our method of classification proved overall favourable for not removing additional aerosol background signatures, but this can be influenced by our aim of study. The main decision to choose an augmented Kent et al. (1993) based curve for cloud classification over a modified T.V. method, was heavily debated during this project. It boiled down to the hazy classification of the *wedge* and *enhanced aerosol* region, example seen in Fig. 4.4-4.5. Keeping the region of *enhanced aerosol* classified as aerosol in Thomasson and Vernier (2013) may be to keep significant ATAL signals in their clean volcanic period of study. However, I observed high amounts of signals in this region that I considered to be cloud characteristics. This hypothesis was drawn from observation and theory that I expect high aerosol extinction signals ($>10^{-2}$ km^{-1}) in one grid (0.5 km) to be accompanied by a surrounding cloud of aerosol signal horizontally and temporally, and I observed a very small amount of high extinction coefficient-signal constellations fulfilling this condition. Ice clouds however, was believed to appear in smaller sizes and able to occupy only few or one grid. The special example of what I considered *enhanced aerosol* is the 1998 and 2017 wildfire smoke in Fig. 5.3c and Fig. A5, where the signal of the smoke-tail aerosol is more linked together in a cluster above the cloud tail. Our results still showed signals of a potential ATAL in June-September with region of high extinction coefficients on the stratospheric tropical region.

After the analysis on the PSC's relationship with the extinction coefficient in our SAGE satellite data was completed, further investigation was suggestable regarding this topic. Our method was purely built from observational methodology between the modelled temperature, Ozone, 525 nm and 1020 nm extinction coefficient relationship, and a supplementary elaboration could possibly give more satisfactory results. However, the PSC potentially have a minor influence on the SAGE III data as it does not exceed over ~60° in latitude, so regarding the newly produced SAGE datasets from 2017 and onwards this is likely not prioritized. Not all signature is removed for the new PSC method seen in Fig. 5.2, but generally a more satisfying result is yielded compared to the Pitts et al. (2009) CALIPSO lidar-based method. I considered the difference of the local sunrise and sunset event for PSC as the atmospheric temperature can vary significantly between them. This could explain why we only see PSC during the typical months of September to October on the southern hemisphere, but also because of the orbital limitation. Supplementary Table A1 and figures on SAGE II Ozone depletion for observational comparison on PSC seen in Appendix.

Fig. 5.3 show a relatively satisfying result when implementing the new combined cloud mask onto the SAGE III dataset. The resulting 2017 521 nm AOD of Fig.5.5 show a

possible forest fire underestimation due to our cloud mask eliminating wildfire enhanced aerosols seen in Fig. 5.3c and Fig. A5. A study by Fromm et al. (2000) suggest an increase is stratospheric aerosol load May to October 1998 from a boreal wildfire in the NH (55-70°N) using multiple observational sources (including SAGE II). I compared the extinction coefficient relationships and saw similarities to the additional aerosol centroid tail seen in Fig. 5.3c, but this cluster is less outlying and not removed in our SAGE II cloud algorithm seen in Fig. A5. So, our resulting NH increase seen in Fig. 5.4 and Fig. A. 3 (September 1998) was concluded to likely be linked to this wildfire event. Adjusting the cloud algorithm for these wildfire events was accessible using a similar method to the T.V. and PSC classification (see Fig. A5) but was not fully tested (every height and months) and therefore not included in the final AOD result. More of these smaller single stratospheric aerosol events are presumably observed in our results but not further investigated in this study but could yield applicable for future research. Wildfire impact on stratospheric radiative forcing is an intriguing subject but limited in our case by the scarce observations from SAGE.

Fig. 5.4-5.7 show that during the volcanic free period of SAGE II 1998-2005 and prior to June 2018 for SAGE III, the total stratospheric AOD suggests a stabilised value at ~0.04-0.06 AOD. As the stratosphere recovers from El Chichón it seems to be dropping back to this background AOD value prior to the Pinatubo eruption 1991, but the Ruiz 1985, and Kelut 1990 eruption likely intercepts and prolongs this recovery period as seen in Fig. 5.5. This background stratospheric AOD-value is recognized to be in par with the volcanic-free periods of total stratospheric AOD in Friberg et al. (2018) ~0.05-0.08 total AOD, and ~0.01-0.03 AOD for the LMS, 380°K - 470°K and 470°K - 40km isentropic layers.

The seasonal AOD changes and aerosol loads in the stratosphere and UTLS Fig. 5.4-5.5 is a relatively undetermined phenomenon but some connections have been drawn in previous studies. The enhancements in NH AOD is proposed to be in parts connected to the Asian summer monsoon, transporting organic and dust aerosol through strong convection to the UTLS (Thomasson and Vernier, 2013; Brühl et al., 2018). Extinction coefficient elevation in the LMS and UTLS is suggested by Brühl et al. (2018) to be greatly influenced by these additional dust and organic aerosols. There is furthermore a seasonal variation and a two-way air mass transport across the tropopause elaborated by Appenzeller and Holton (1996), proposing e.g. how the mass and thickness of the LMS increases during winter time in the NH. These intricate dynamic flows over isentropic surfaces could explain how aerosol loads additionally changes with seasonality. Together, this truly illustrates the difficulties of parameterizing aerosols in modelling, as you must include processes from synoptic/meso-scale flow, convection (meteorology) and volcanic activity to micro-scale processes like e.g. nuclei-interactions and cloud formation. However, our aim to gain further understanding to these processes during this project proved rewarding.

The GloSSAC method following the Pinatubo eruption is using two longer wavelengths from additional satellites HALOE (3.4 μm) and CLEAS (12.82 μm), elaborated in

Thomasson et al. (2018). This method is desired to be tested and implemented into our dataset for future studies. Further improvement, suggested by Bauman et al. (2003), which implies that the mount Hudson August eruption in 1991 is more prominent when implementing the longwave CLEAS extinction data as SAGE II is limited in this period from Pinatubo (see Fig. A2). GloSSAC furthermore uses a 5° mean latitude values for the extinction coefficient (I use 1°) and they later extrapolate each height-level seen in Thomasson et al. (2018). I expect this difference of data compilation is causing their AOD data curves to appear smoother in Fig. 5.7, while our more jagged AOD curve reveals possible drastic temporal changes like e.g. the Kelut eruption 1990 and the wildfires of 1998. I do raise some question to their extrapolation near the tropopause as we observed a large zonal and meridional variation in our TP height. This implies that they may inter/extrapolate tropospheric data (e.g. at 10 km in the tropics) into the stratosphere (at 10 km in > mid-latitudes) which could carry a change of characteristics. I only inter/extrapolate on isentropic surfaces which may potentially be better for isolating stratospheric airmasses. But since our TP is static, I do not presume to call our method more qualified. Worth noting that the GloSSAC data of volcanic stratospheric influence will act as the archetype for parameterising the effects into IPCC's next model CMIP 6 (Zanchettin et al., 2016).

Lastly, the provided wavelength uncertainties of SAGE II and III channels may include some further understanding of the confidence to each event and their respective AOD. This could prove consequential for later analysis and is sought for establishing and quantifying AOD to radiative forcing in future studies. I also took note to the modelled static tropopause provided in the SAGE II datasets which I subsequently used for our definition of ExTL, LMS and the total stratosphere. For future implementation I also wish to compare our TP to an adjacent ECMWF's dynamic tropopauses at a specific time, latitudes and longitudes given in the SAGE II data to check for potential deviation in our static tropopause. In GloSSAC, they implement just this using MERRA and a WMO tropopause for SAGE II (Thomasson et al. 2018).

7. Conclusions

The process of applying and comparing different cloud algorithms gave us a well-reasoned concept of the two SAGE channels 525 nm and 1020 nm extinction coefficient behaviour and their relationship. The considered cloud and aerosol centroid signals have a general nature in our observations that I can use to classify my data in a practical sense. Discovering the appearance and conduct of volcanic and forest fire aerosol in our data will provide a good comparison scheme to other observational data such as lidar measurements. This could prove useful for later quantification of impact for these phenomena. Evaluating the Kent et al (1993) and Thomasson and Vernier (2013) method results of cloud removal generated the intention for further improvement, with the aim not to under/overestimate a stratospheric aerosol event. This could be achieved over our study-period apart from the Pinatubo eruption. Our method of PSC removal I found more agreeable to uniform observations in the monthly mean data plots, but the overall influence on the global AOD remains small for PSC but could carry a larger influence in local polar studies. The mentioned potential forest fire events have an observable impact on the stratospheric extinction and is desired to peruse further as these phenomena is not mentioned in Thomasson et al. (2018).

The new produced method was also expected to give more satisfactory results when later classifying clouds, volcanic and forest aerosols for SAGE III data. The SAGE III information is newly acquired from fresh datasets (< September 2019) and further examination to our cloud algorithm and resulting extinction coefficient to recent events is an attractive study, e.g. the current massive Australian summer 2019/2020 forest fire.

Compiling our results to seasonal and zonal stratospheric aerosol optical depths was key to understand the important steps in our methodology. Reviewing the cloud mask and extrapolation/interpolation of data with comparison to the Thomasson et al. (2018) GloSSAC data directed us towards the most satisfactory method, with some missing exceptions due to availability and project time. Recent SAGE III comparison to the CALIPSO data evaluated in Friberg et al. (2018), is likely beneficial for future cloud/aerosol interpretation and composition to SAGE II and SAGE III.

References

Ahrens, C.D. *Meteorology Today: An Introduction to Weather and the Environment*. Belmont, USA, 11th edition, pp. 170-182 527-546, 2008.

Albrecht, B.A., Aerosols, Cloud Microphysics, and Fractional Cloudiness. *Science*. 245, 1227–1230. 1989

Appenzeller, Christof & Holton, James & Rosenlof, K., *Seasonal Variation of Mass Transport Across the Tropopause*. J. Geophys. Res. doi:101.10.1029/96JD00821, 1996.

Bauman, J. J., Russell, P. B., Geller, M. A., and Hamill, P.: *A stratospheric aerosol climatology from SAGE II and CLAES measurements: 1. Methodology*, J. Geophys. Res.-Atmos., 108, 4382, doi:10.1029/2002jd002992, 2003.

Brühl, C., Schallock, J., Klingmüller, K., *Stratospheric aerosol radiative forcing simulated by the chemistry climate model EMAC using Aerosol CCI satellite data*. Atmos. Chem. Phys., 18(17), 12845–12857. doi:10.5194/acp-18-12845-2018, 2018.

Damadeo, R. P., Zawodny, J. M., Thomason, L. W., Iyer, N.: *SAGE version 7.0 algorithm: application to SAGE II*, Atmos. Meas. Tech., 6, 3539–3561, doi:10.5194/amt-6-3539-2013, 2013.

Friberg, J., Martinsson, B.G., Anderson, S.M., and Sandvik, O., *Volcanic impact on the climate – the stratospheric aerosol load in the period 2006-2015*, Atmos. Chem. Phys., 18, 11149–11169, doi:10.5194/acp-18-11149-2018, 2018.

Fromm, M., Alfred, J., *Observation of boreal fire smoke in the stratosphere by POAM III, SAGE II, and lidar in 1998*, Geophys., 27, 1407-1410, doi:10.1029/1999GL011200, 2000.

Fueglistaler, S., Dessler, A. E., Dunkerton, T. J., Folkins, I., Fu, Q., and Ote, P. W.: *Tropical tropopause layer*, Rev, Geophys., 47, RG1004, doi:10.1029/2008RG000267 , 2009.

Gettelman, A., P. Hoor, L. L. Pan, W. J. Randel, M. I. Hegglin, and T. Birner (2011), *The extratropical upper troposphere and lower stratosphere*, Rev. Geophys., 49, RG3003, doi:10.1029/2011RG000355.

Global Volcanism Program, 2013. Volcanoes of the World, v. 4.8.4. Venzke, E (ed.). Smithsonian Institution., doi:10.5479/si.GVP.VOTW4-2013 , [Accessed: 29 Dec 2019].

Holton, J. Hakim, G. *An Introduction to Dynamic Meteorology*, Volume 88, 5th edition, pp. 50-254, 2012.

IPCC: Climate Change 2013: *The Physical Science Basis. Contribution of Working Group I to the Fifth Assessment Report of the Intergovernmental Panel on Climate Change*, edited by: Stocker, T. F., Qin, D., Plattner, G.-K., Tignor, M., Allen, S. K., Boschung, J., Nauels, A., Xia, Y., Bex, V., and Midgley, P. M., Cambridge University Press, Cambridge, UK and New York, NY, USA, 1535 pp., doi:10.1017/CBO9781107415324 , 2013.

Kent, G. S., M.P. McCormick, and S. K. Schaffner, Global optical climatology of the free tropospheric aerosol from 1.0-/am satellite occultation measurements, J. Geophys. Res., 96, 5249-5267, 1991.

Kent, G. S., Winker, D. M., Osborn, M. T., McCormick, M. P., and Skeens, K. M.: *A model for the separation of cloud and aerosol in SAGE II occultation data*, J. Geophys. Res., 98, 20725–20735, 1993.

Khaykin, S. M., Godin-Beekmann, S., Hauchecorne, A., Pelon, J., Ravetta, F., Keckhut, P., *Stratospheric Smoke With Unprecedentedly high Backscatter Observed by Lidars Above Southern France*, Geophys, Vol 45, Issue 3, 1195-1700, doi:10.1002/2017GL076763, 2018

Lin, P. and Fu, Q.: *Changes in various branches of the Brewer–Dobson circulation from an ensemble of chemistry climate models*, J. Geophys. Res.-Atmos., 118, 73–84, doi:10.1029/2012JD018813 , 2013.

McCormick, M. P., *SAGE II: An overview*, Adv. Space Res., 7(3), 219– 226, doi:10.1016/0273-1177(87)90151-7 1987.

NASA: Atmospheric Science Data Center, Project SAGE II, https://eosweb.larc.nasa.gov/project/sage2, [Accessed: 25 Nov 2019].

Pitts, M. C., Poole, L. R., and Thomason, L. W.: *CALIPSO polar stratospheric cloud observations: second-generation detection algorithm and composition discrimination*, Atmos. Chem. Phys., 9, 7577–7589, doi:10.5194/acp-9-7577-2009 , 2009.

Thomason, L. W., Burton, S. P., Luo, B.-P., and Peter, T.: *SAGE II measurements of stratospheric aerosol properties at non-volcanic levels*, Atmos. Chem. Phys., 8, 983–995, doi:10.5194/acp-8-983-2008, 2008.

Thomason, L. W. and Vernier, J.-P.: *Improved SAGE II cloud/aerosol categorization and observations of the Asian tropopause aerosol layer: 1989–2005*, Atmos. Chem. Phys., 13, 4605–4616, doi:10.5194/acp-13-4605-2013, 2013.

Thomason, L. W., Ernest, N., Millán, L., Rieger, L., Bourassa, A., Vernier, J.-P., Manney, G., Luo, B., Arfeuille, F., and Peter, T.: *A global space-based stratospheric aerosol climatology: 1979–2016*, Earth Syst. Sci. Data, 10, 469–492, doi:10.5194/essd-10-469-2018, 2018.

Twomey, S. A. *The nuclei of natural cloud formation. Part II: The supersaturation in natural clouds and the variation of cloud droplet concentrations*. Geofis. Pure Appl. Vol.43, 227–242. 1959.

Wallace, J.M., Hobbs, P.V., *Atmospheric Science: An introductory Survey*, Second Edition, Elsevier Academic Press, London, pp. 113-371, 2006.

Yue, G. K., *Wavelength dependence of aerosol extinction coefficient for stratospheric aerosols*, J. Clim. Appl. Meteorol., 25, 1775-1779, 1986.

Yue, G. K., C.-H. Lu, and P.-H. Wang, *comparing aerosol extinctions measured by Stratospheric Aerosol and Gas Experiment (SAGE) II and III satellite experiments in 2002 and 2003*, J. Geophys. Res., 110, D11202, doi:10.1029/2004JD005421 , 2005.

Zambri, B., Robock, A., Mills, M. J., & Schmidt, A., *Modeling the 1783–1784 Laki eruption in Iceland: 2. Climate impacts*, Journal of Geophysical Research: Atmospheres, 124, 6770– 6790. doi:10.1029/2018JD029554, 2019.

Zanchettin, D., Khodri, M., Timmereck, C., *The model intercomparison project on the climatic response to volcanic forcing (VolMIP): Experimental design and forcing input data for CMIP6,* Geosci. Model Dev., 9, 2701–2719, doi:10.5194/gmd-9-2701-2016, 2016.

Appendix

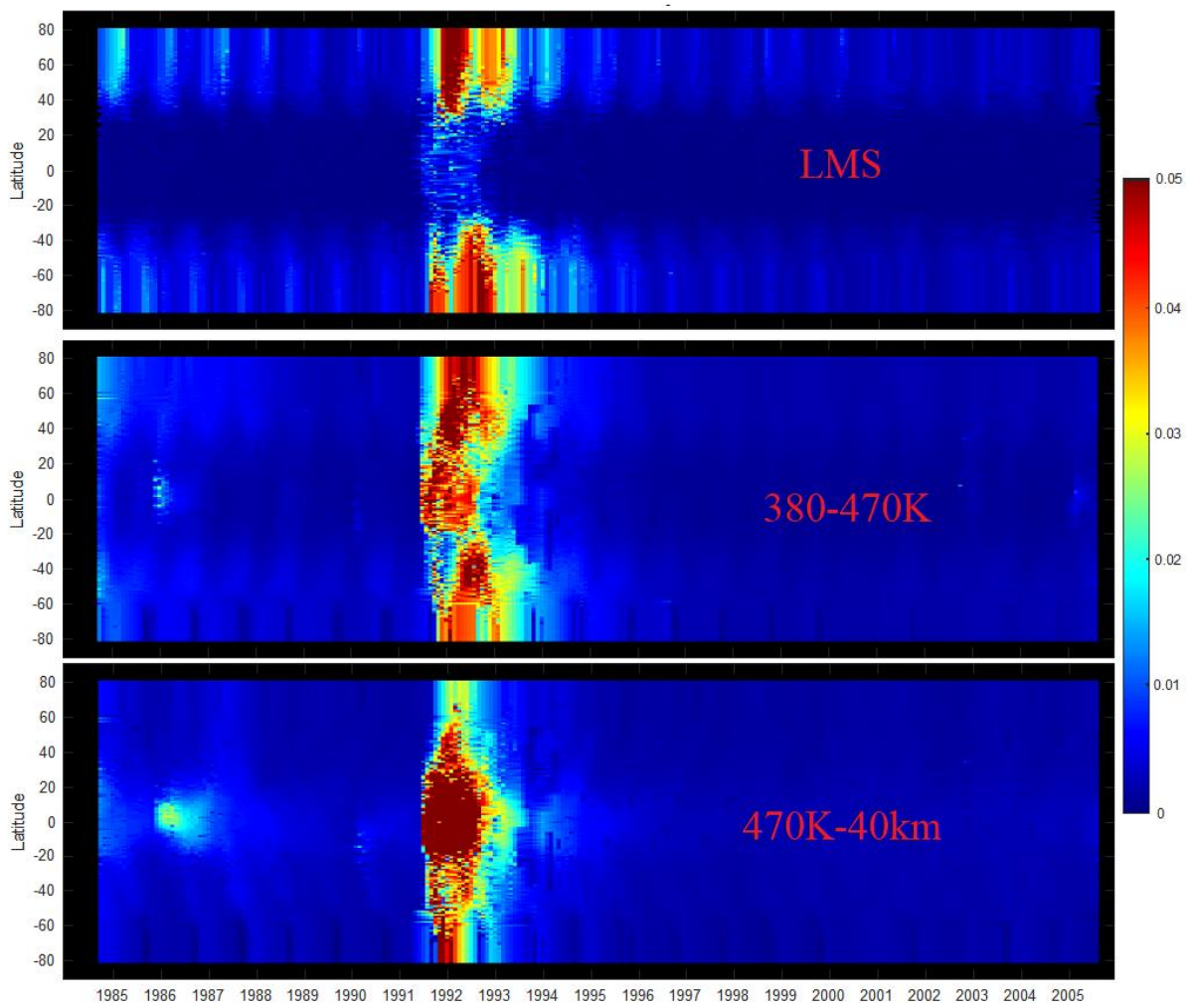

Figure A1: The resulting cloud-removed SAGE II stratospheric zonal mean 525 nm AOD of the LMS, 380°K-470°K and 470°K – 40 km after they are individually inter/extrapolated. Fig. 5.4 show total stratospheric AOD which is the sum of these three layers.

Table A1: The Cloud algorithm combined years of computation with δ and k_a values used in Section 4.3 of modified Eq. 6. for PSC classification (red line in Fig. 4.6).

Years in cloud algorithm	delta (δ)	k_a of 1020 nm (km^{-1})
1984 (Oct-Dec)	*X*	*X*
1985	1.5	10^{-4}
1986-1987	2.0	$8 * 10^{-5}$
1988-1991(-Jun)	2.0	$8 * 10^{-5}$
1994	1.2	$2 * 10^{-4}$
1995	1.2	$2 * 10^{-4}$
1996-1998	1.5	k_a
1999-2005(-Aug)	1.5	k_a

1984 and 1991-1993 is excluded from Table 1 as they do not contain data within the reasonable frame for PSC signal observation. The centroid value k_a from Eq. 6 can be used for the PSC function in the most volcanic free period of 1996-1998 and 1999-2005. Series of years are selected with respect to method related to Fig .4.3.

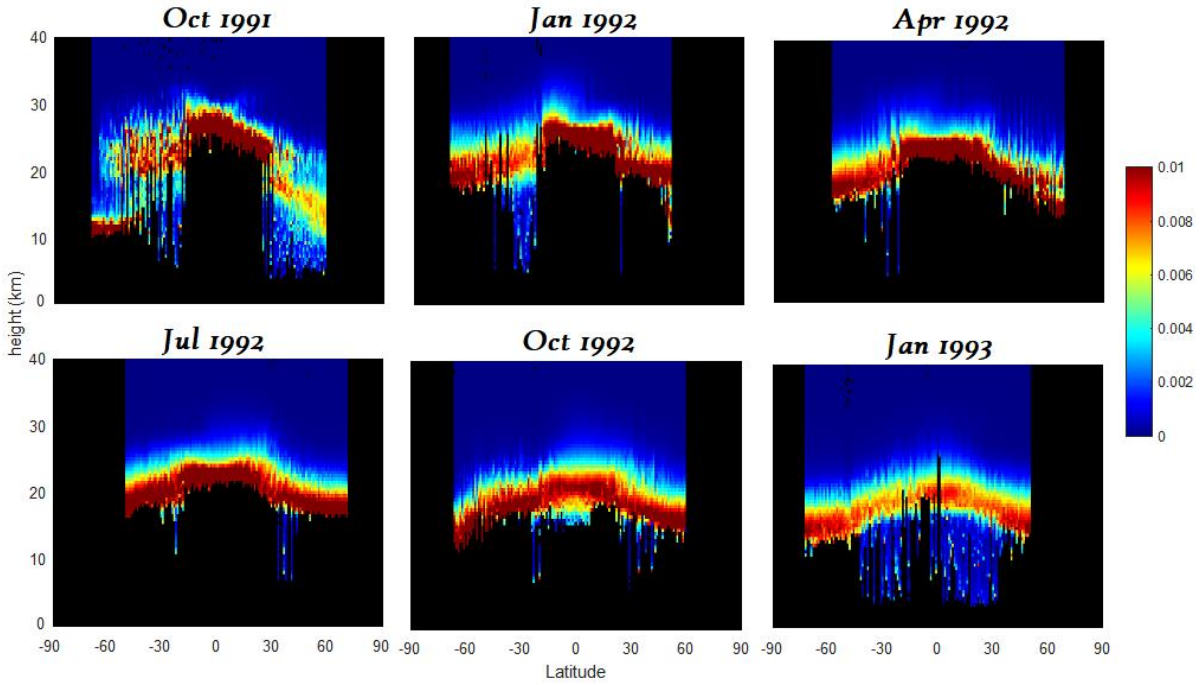

Figure A2: Examples of monthly mean SAGE II 525 nm Extinction coefficient (km^{-1}) following the mt. Pinatubo eruption June 1991 where large portions of extinction values have been removed in the v.7.0 SAGE II dataset when exceeding line of sight AOD of ~7.

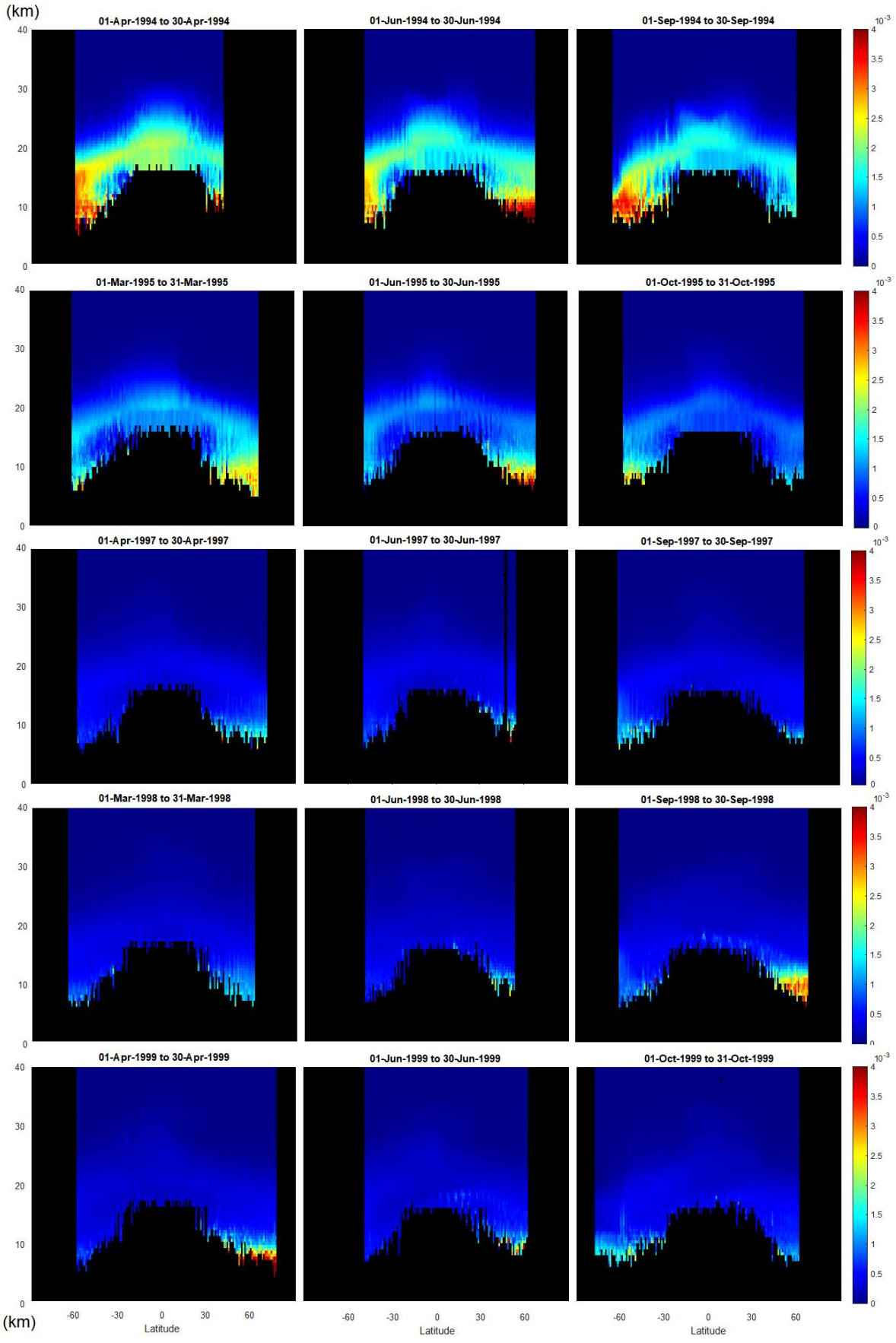
(km)
01-Apr-1994 to 30-Apr-1994
01-Jun-1994 to 30-Jun-1994
01-Sep-1994 to 30-Sep-1994
01-Mar-1995 to 31-Mar-1995
01-Jun-1995 to 30-Jun-1995
01-Oct-1995 to 31-Oct-1995
01-Apr-1997 to 30-Apr-1997
01-Jun-1997 to 30-Jun-1997
01-Sep-1997 to 30-Sep-1997
01-Mar-1998 to 31-Mar-1998
01-Jun-1998 to 30-Jun-1998
01-Sep-1998 to 30-Sep-1998
01-Apr-1999 to 30-Apr-1999
01-Jun-1999 to 30-Jun-1999
01-Oct-1999 to 31-Oct-1999
0
10
20
30
40
-60
-30
0
30
60
Latitude
10^{-3}
0
0.5
1
1.5
2
2.5
3
3.5
4

Figure A3: Examples of monthly mean SAGE II 525 nm Extinction coefficient (km^{-1}) excluding tropospheric values using SAGE II modelled height of tropopause, from months post Pinatubo and for observations of a seasonal trend in the LMS-470°K.

The supplementary Ozone schematic in Fig. A4 is made to try to illustrate how PSC may show depleting signatures on the NH contra to the SH, but no such signature in the polar NH extinction coefficient or O_3 plotted data were detected.

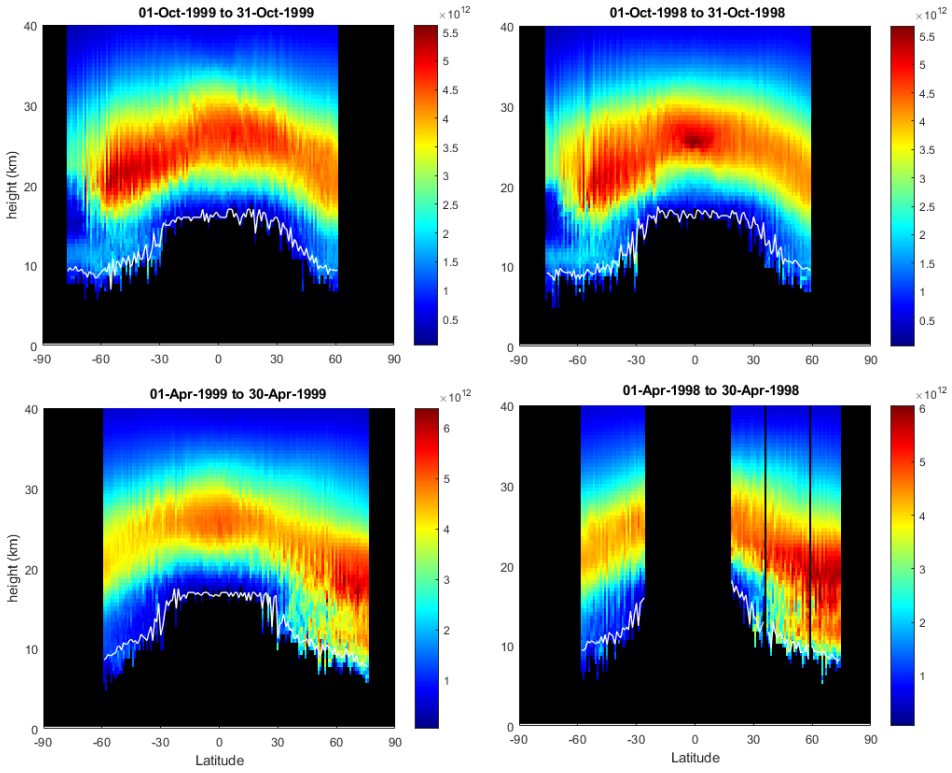

Figure A4: Examples of monthly mean SAGE II stratospheric Ozone number density (cm^{-3}) for two October months of observed PSC in the SH vs two April months for NH comparison when SAGE II captures the high latitudes (>70°) respectively. White line represents zonal mean tropopause.

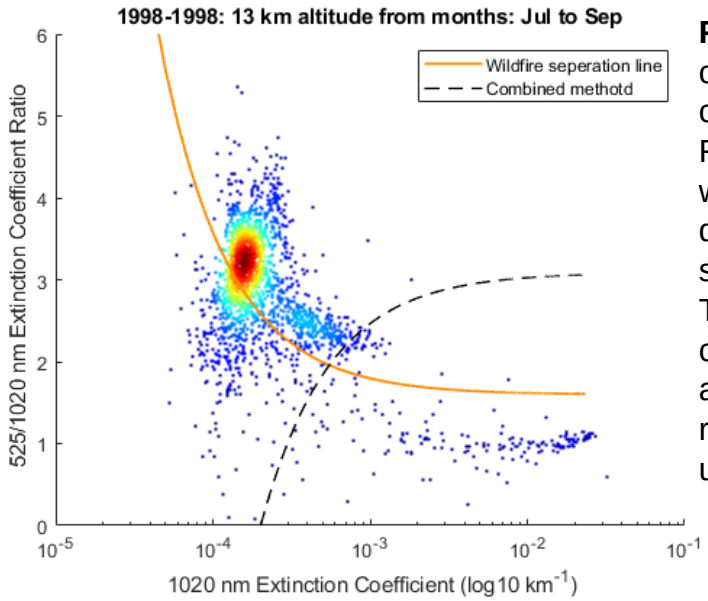

Figure A5: The extinction coefficient cloud and wildfire smoke classification scatterplot for the Fromm et al. (2000) proposed NH wildfire in 1998 and what the distinct secondary cloud-tail signature we related to Fig. 5.3c. The *wildfire separation line* classifies all values overhead as aerosol, but original cloud tail remains cloud classified underneath.